HHS Public Access

Author manuscript

Cell. Author manuscript; available in PMC 2021 October 29.

Published in final edited form as:

Cell. 2020 October 29; 183(3): 650–665.e15. doi:10.1016/j.cell.2020.09.022.

Endocannabinoids Inhibit the Induction of Virulence in Enteric Pathogens

Melissa Ellermann[1,2], **Alline R. Pacheco**[1,2], **Angel G. Jimenez**[1,2], **Regan Russell**[1,2], **Santiago Cuesta**[1,2], **Aman Kumar**[1,2], **Wenhan Zhu**[1], **Gonç alo Vale**[3], **Sarah A. Martin**[4], **Prithvi Raj**[5], **Jeffrey McDonald**[3], **Sebastian E. Winter**[1], **Vanessa Sperandio**[1,2,6,*]

[1]Department of Microbiology, UT Southwestern Medical Center, Dallas, TX 75390, USA

[2]Department of Biochemistry, UT Southwestern Medical Center, Dallas, TX 75390, USA

[3]Center for Human Nutrition, UT Southwestern Medical Center, Dallas, TX 75390, USA

[4]Department of Molecular Genetics, UT Southwestern Medical Center, Dallas, TX 75390, USA

[5]Microbiome Research Lab, Department of Immunology, UT Southwestern Medical Center, Dallas, TX 75390, USA

[6]Lead Contact

SUMMARY

Endocannabinoids are host-derived lipid hormones that fundamentally impact gastrointestinal (GI) biology. The use of cannabis and other exocannabinoids as anecdotal treatments for various GI disorders inspired the search for mechanisms by which these compounds mediate their effects, which led to the discovery of the mammalian endocannabinoid system. Dysregulated endocannabinoid signaling was linked to inflammation and the gut microbiota. However, the effects of endocannabinoids on host susceptibility to infection has not been explored. Here, we show that mice with elevated levels of the endocannabinoid 2-arachidonoyl glycerol (2-AG) are protected from enteric infection by Enterobacteriaceae pathogens. 2-AG directly modulates pathogen function by inhibiting virulence programs essential for successful infection. Furthermore, 2-AG antagonizes the bacterial receptor QseC, a histidine kinase encoded within the core Enterobacteriaceae genome that promotes the activation of pathogen-associated type three secretion systems. Taken together, our findings establish that endocannabinoids are directly sensed by bacteria and can modulate bacterial function.

Graphical Abstract

*Correspondence: vanessa.sperandio@utsouthwestern.edu.

AUTHOR CONTRIBUTIONS

M.E. designed and conducted experiments and wrote the paper, A.R.P. designed and conducted experiments, A.G.J., R.M.R., A.K., and S.C. conducted experiments, W.Z. analyzed data, G.V., S.A.M., and P.J. conducted experiments and analyzed data, J.M. designed experiments, S.E.W. analyzed data, and V.S. supervised all experiments, analyzed data, and wrote the paper.

SUPPLEMENTAL INFORMATION

Supplemental Information can be found online at https://doi.org/10.1016/j.cell.2020.09.022.

DECLARATION OF INTERESTS

The authors declare no competing interests.

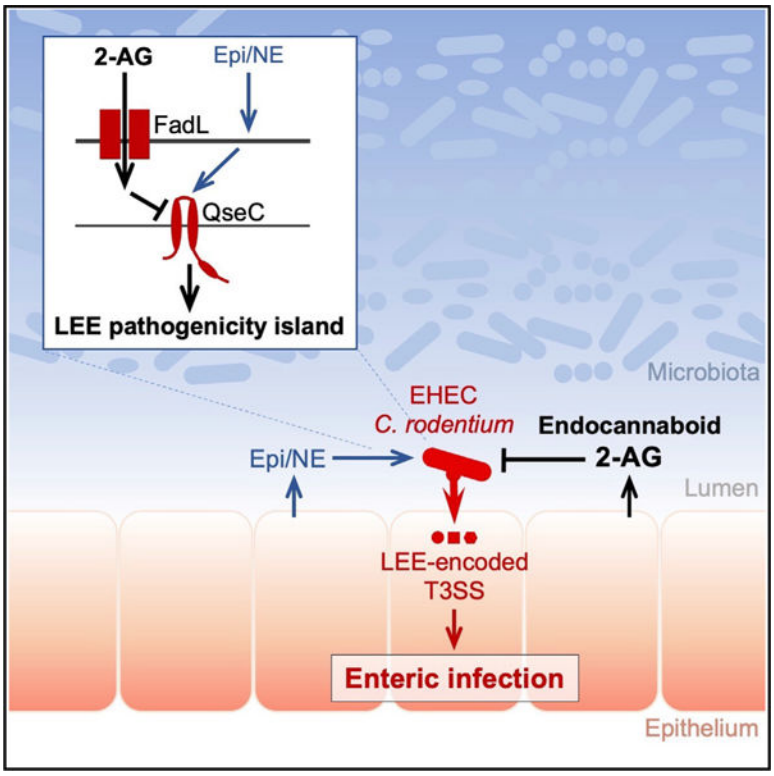

In Brief

The endocannabinoid hormone 2-AG protects mice from enteric bacterial infection via inhibition of pathogen virulence programs, resulting in reduced pathogen burden and attenuated colitis in mice with increased 2-AG levels.

INTRODUCTION

The gastrointestinal (GI) tract harbors a complex community of endogenous microbes essential to maintain intestinal homeostasis (Sartor and Wu, 2017). The metabolic and physiological activities of host and microbial cells generate an intestinal microenvironment with a diverse milieu of small molecules. Invading bacterial pathogens evolved mechanisms to sense many of these chemical cues. They integrate this biochemical information into the regulation of key virulence-associated pathways and signaling networks to successfully colonize the intestine and allow rapid niche formation, replication, and subsequent transmission to the next host (Bäumler and Sperandio, 2016).

Intestinal pathogens, such as enterohemorrhagic *Escherichia coli* (EHEC) and the murine pathogen *Citrobacter rodentium* (CR), colonize the large intestine by attaching to the colonic epithelium, which enables pathogen replication and results in the effacement of the microvilli and actin rearrangement forming pedestal-like structures known as AE lesions leading to the development of diarrhea. AE pathogens harbor a pathogenicity island named the locus of enterocyte effacement (LEE), which is essential for AE lesion formation. The LEE encodes a type 3 secretion system (T3SS), a molecular syringe that injects bacterial

proteins known as effectors into host cells that enables the establishment of a replicative niche (Knutton et al., 1989; Kaper et al., 2004). Mutants in the LEE-encoded adhesin intimin, components of the T3SS, or key effectors are unable to form AE lesions on epithelial cells (Deng et al., 2004). Other enteric pathogens such as *Salmonella enterica* serovar Typhimurium also utilize T3SSs to modify their local environment to promote disease (Barthel et al., 2003; Hapfelmeier et al., 2004; Santos et al., 2001). *S. typhimurium* harbors the *Salmonella* pathogenicity islands 1 (SPI-1) and SPI-2, which encode T3SSs that enable intestinal epithelial invasion and intracellular replication, respectively (Galán and Curtiss, 1989; Ochman et al., 1996).

Specific chemical signals in the intestine modulate the expression and function of T3SSs (Kumar et al., 2019). AE pathogens and *S. typhimurium* sense the host neurotransmitters epinephrine (epi) and norepinephrine (NE) via the bacterial adrenergic receptor QseC, a histidine kinase (HK), encoded within the core genomes of γ-Proteobacteria (Clarke et al., 2006; Rasko et al., 2008; Moreira et al., 2010; Rooks et al., 2017). Epi/NE engagement with QseC activates intracellular signaling cascades that regulate bacterial physiology, behavior, function, and virulence (Sperandio et al., 2002; Clarke and Sperandio, 2005; Hughes et al., 2009). In AE pathogens, QseC activation promotes increased expression of *ler*, the master transcriptional regulator of the LEE operons (Clarke et al., 2006). In contrast, the QseC synthetic inhibitor LED209 attenuates the virulence of EHEC and CR (Rasko et al., 2008; Curtis et al., 2014). Transcription of the master regulators of SPI-1 and SPI-2 in *Salmonella* is also activated upon epi/NE binding to QseC (Moreira et al., 2010). Thus, QseC-mediated sensing of the local intestinal environment exacerbates pathogen infection through the upregulation of virulence programs.

The mammalian endocannabinoid system is composed of lipid-based signaling molecules known as endocannabinoids, which modulate GI physiology and immunity (Cani et al., 2016; Turcotte et al., 2015). The two major host endocannabinoids, anandamide and 2-arachidonoyl glycerol (2-AG), are synthesized through the lipolysis of host membrane phospholipid precursors and then activate their cognate G-protein-coupled receptors CB1 and CB2 to stimulate a cellular response (Devane et al., 1992; Bisogno et al., 1997; Deutsch and Chin, 1993; Mechoulam et al., 1995). Membrane-associated host lipases degrade endocannabinoids to terminate signaling (Dinh et al., 2002; Bisogno et al., 1997; Deutsch and Chin, 1993; Blankman et al., 2007). Recent reports showed that lipases encoded within bacterial genomes can also hydrolyze 2-AG *in vitro* (Côtes et al., 2007; Dhouib et al., 2010). Thus, bacteria may sense and respond to endocannabinoids in the gut environment, which could alter outcomes of infection.

Host endocannabinoid signaling has been reported to promote anti-inflammatory responses, including in chemical and non-infectious models of intestinal inflammation (Massa et al., 2004; Engel et al., 2008, 2010; Romano et al., 2013; Shamran et al., 2017; D'Argenio et al., 2006; Andrzejak et al., 2011; Storr et al., 2008; Zhao et al., 2017; El Bakali et al., 2014; Leinwand et al., 2017; Alhouayek et al., 2011; Turcotte et al., 2015). However, the effects of endocannabinoids on intestinal infection have not been explored. Here, we report that mice with elevated levels of the endocannabinoid 2-AG exhibit attenuated disease when infected with the AE pathogen CR or *S. typhimurium*. We further show that 2-AG directly modulates

the virulence of pathogenic Enterobacteriaceae by inhibiting the activation of the provirulence receptor QseC. This dampens the deployment of their T3SSs essential for successful pathogen colonization, replication, and disease causation. Collectively, our findings suggest that the anti-virulence effects of 2-AG on pathogen function contribute to the protection against enteric infection observed in mice with elevated 2-AG.

RESULTS

Mice with Elevated Levels of the Endocannabinoid 2-Arachidonoyl Glycerol Are Protected against Enteric Infection

To establish whether endocannabinoids modulate infectious disease, we investigated susceptibility to infection with the murine AE pathogen CR in mice with elevated 2-AG. The enzyme monoacylglycerol lipase (Mgll) degrades 2-AG into arachidonic acid (AA) and glycerol (Figure 1A; Dinh et al., 2002, 2004). *Mgll* knockout (*Mgll* KO) mice have increased 2-AG levels in various organs including the colon during homeostasis and infection (Figure 1B; Schlosburg et al., 2010; Taschler et al., 2015). We infected *Mgll* KO and wild-type (WT) mice littermate controls with CR to compare the effects of different levels of host 2-AG on intestinal bacterial infection. *Mgll* KO mice developed significantly attenuated intestinal disease in response to CR infection as assessed by gross pathology at days 7 and 10 (Figure 1C) and histology at day 10 (Figures 1D–1F and 1H). Crypt hyperplasia, a hallmark of CR infection (Luperchio and Schauer, 2001), was decreased in the ceca and distal colons of *Mgll* KO mice (Figures 1F and 1H) where CR attaches to the colonic epithelium (Mullineaux-Sanders et al., 2019). Notably, a larger proportion of *Mgll* KO mice (85.7% at day 7, 100% at day 10) exhibited mild disease (score of 4 or less) compared to *Mgll* WT mice (33.3% at day 7, 11.1% at day 10) (Figure 1C). The attenuated pathology observed in *Mgll* KO mice corresponded with decreased colonic expression of several proinflammatory cytokines, including *Nos2*, *Lcn2*, and *Mip2a*, which positively correlate with CR disease progression and severity (Figures 1G and S1A–S1C). Moreover, in contrast to WT mice, the expression of these inflammation markers remained unaltered during the course of infection in *Mgll* KO mice (Figures 1G, S1A, and S1B). These data demonstrate that *Mgll* KO mice develop less severe intestinal disease in response to CR infection.

We then hypothesized that 2-AG mediates the protective effects against CR infection in *Mgll* KO mice. However, because other monoacylglycerols (MAGs) can serve as substrates for *Mgll*, genetic ablation of *Mgll* may potentially alter the profile of other biologically active lipids in addition to 2-AG (Nomura et al., 2010). Moreover, abrogation of 2-AG hydrolysis by Mgll can decrease the generation of AA in certain tissues, which can in turn modulate inflammation (Nomura et al., 2008; Schlosburg et al., 2010; Long et al., 2009). We therefore assessed whether genetic ablation of *Mgll* alters colon concentrations of AA and other MAG substrates of *Mgll.* Congruent with previous reports, we found that AA was not increased in the colons of *Mgll* KO mice, including in mice infected with CR (Figure S1D; Nomura et al., 2011). Colonic levels of other detectable MAGs also remained unchanged in PBS-treated or infected *Mgll* WT and KO mice (Figures S1E and S1F). These data suggest that *Mgll* deficiency primarily alters colonic 2-AG levels and does not impact the levels of AA or other

MAGs in the colon. These findings indicate that elevated 2-AG likely mediates the protective effects against enteric infection observed in *Mgll* KO mice.

C. rodentium Colonization of Colonic Tissues Is Attenuated in Mice with Increased 2-AG

Development of more severe intestinal pathology during infection can occur as a result of increased pathogen virulence potential, which enables enhanced pathogen replication, and can exacerbate inflammation and disease. We then determined whether the attenuated pathology observed in infected *Mgll* KO mice corresponds with reduced intestinal burdens of CR. Fecal shedding of CR were not significantly different between *Mgll* WT or KO mice at days 1, 2, 4, and notably at day 7 post-infection (Figure 2A). However, by day 10 (peak of disease in this murine model), fecal loads of CR were significantly decreased in *Mgll* KO mice relative to WT controls (Figures 2A and 2B). This difference seemed to be primarily driven by the lack of detectable CR colony-forming units (CFUs) in fecal samples collected from a subset of *Mgll* KO mice (CR-positive cultures in *Mgll* WT versus KO: 94.4% versus 57.1% of mice).

We next assessed the extent of CR colonization in cecal and distal colon tissues because both sites serve as replicative niches for CR in the murine gut where consequent tissue damage occurs (Mullineaux-Sanders et al., 2019). *Mgll* KO mice exhibited reduced CR loads in cecal tissues at days 7 and 10 (Figures 2C and 2D) and in distal colon tissues at day 10 (Figure 2E). As observed in stools, differences in CR colonization of the cecum and distal colon were primarily driven by an increased proportion of *Mgll* KO mice that were negative for CR by culture (Figures 2B–2E). By day 10, live CR was not recoverable from colon tissues in the majority of *Mgll* KO mice, whereas nearly 100% of *Mgll* WT mice remained infected (Figures 2D and 2E). Moreover, CR was not detectable in the ceca of a subset of *Mgll* KO mice that continued to shed CR in feces, a phenomenon that was not observed in *Mgll* WT mice (Figure 2F). Sex also seemed to contribute to the variability in CR fecal shedding and tissue colonization observed in *Mgll* KO mice (Figures S2A–S2C). A greater proportion of female *Mgll* KO mice were culture negative for CR compared to males, which corresponded with a trend toward increased levels of colonic 2-AG (Figure S2D). These data suggest that *Mgll* KO mice with elevated 2-AG clear the CR infection earlier than *Mgll* WT mice, which corresponds with the attenuated inflammation and pathology observed in *Mgll* KO mice.

C. rodentium Infection Is Attenuated with Mgll Blockade

Next, we investigated whether *Mgll* KO mice, which have chronically altered endocannabinoid tone, showed any overt changes on immune function. Genetic ablation of *Mgll* modestly alters the basal expression of a few markers of immune function, notably *Lcn2*, *Il10*, and *Il12b*, in the colons of untreated adult mice (Figures S2E and S2F), which in turn may play a role in modulating the host response to enteric infection. We therefore also employed a pharmacological approach to increase colonic levels of 2-AG in WT mice using the Mgll inhibitor JZL184 as previously reported (Long et al., 2009; Alhouayek et al., 2011; Taschler et al., 2015). Similarly to *Mgll* KO mice, CR cecal burdens were decreased in WT mice treated with JZL184 compared to vehicle controls, which corresponded with attenuated cecal pathology (Figures 2G, 2H, and S2G–S2I). Moreover, as observed with *Mgll* KO mice,

at least 50% of JZL184-treated mice were negative for CR by cecal culture, despite continuing to shed CR in feces at days 7 and 10 post-infection (Figures 2G and S2G–S2I). In contrast, most vehicle-treated mice remained colonized with *CR* (Figures 2G and S2G–S2I). Notably, JZL184 did not alter CR burdens in cecal tissues or feces and had no impact on cecal pathology in *Mgll* KO mice (Figures 2I, 2J, S2I, and S2J), which is likely indicative of minimal off-target effects of the inhibitor in our CR infection model. These data suggest that increased 2-AG as a result of Mgll dysfunction attenuates CR infection, which corresponds with faster clearance of the pathogen, and attenuated disease.

Endocannabinoid signaling mediated by 2-AG manifests through the activation of the host cannabinoid receptors CB1 or CB2, which stimulates complex intracellular signaling cascades that modulate GI physiology and immunity (Leinwand et al., 2017b; Taschler et al., 2017). However, chronic blockade of Mgll results in the desensitization of the CB1 receptor in the gut (Schlosburg et al., 2010; Taschler et al., 2015). Moreover, because 2-AG seems to primarily modulate immune function through its interactions with CB2 to impart its anti-inflammatory effects (Turcotte et al., 2016), we reasoned that 2-AG may attenuate infectious disease by activating CB2 receptors. To address this, we next investigated whether CB2 blockade with the inhibitor AM630 can reverse the protective effects of JZL184 observed with CR infection. CR fecal shedding, colonization of cecal tissues, and corresponding cecal pathology were all comparable between WT mice that were administered JZL184 or co-administered JZL184 and AM630 (Figures 2G, 2H, and S2G). These findings suggest that the protective effects of 2-AG on CR infection are not mediated through the engagement of the host CB2 receptor.

Attenuated Infection in *Mgll* KO Mice Is Unlikely Mediated through the Microbiota

Because endocannabinoid tone can affect microbiota composition (Everard et al., 2013; Cani et al., 2016), we next assessed whether compositional or functional changes to the microbiota may explain the attenuated CR infection observed in *Mgll* KO mice. Microbiota community profiling revealed that prior to infection with CR, the microbiotas between WT and *Mgll* KO mice did not significantly differ in composition (Figures S3A and S3B). To determine whether functional differences in the microbiota that may occur as a result of elevated 2-AG mediates protection against enteric infection, we performed fecal microbiota transplantation (FMT) experiments. Germ-free WT recipients were engrafted with the microbiota from *Mgll* WT or KO donors and then subjected to CR infection. Pathogen loads in feces and colon tissues and corresponding colon pathology did not differ between recipients of the *Mgll* WT or KO FMT (Figures S3C–S3F). Together, these findings suggest that the microbiota unlikely mediates the faster clearance of CR and attenuated disease observed in *Mgll* KO mice (Figures S1E and S1F).

The Endocannabinoid 2-AG Directly Inhibits Virulence-Associated Functions in Intestinal AE Pathogens

AE pathogens such as CR and EHEC harbor the LEE pathogenicity island that is essential for successful colonization of the intestines and consequent induction of disease (Figure 3A). The LEE-encoded T3SS enables AE pathogens to inject their effectors into colonocytes (Figure 3B; Knutton et al., 1989; Kaper et al., 2004). Genetic inactivation of the LEE

abrogates the formation of AE lesions on epithelial cells, colonization of the gut, and consequent disease and thus renders these mutants avirulent (Kaper et al., 2004; Deng et al., 2004). Moreover, the transcriptional expression of LEE-encoded genes in CR positively correlates with its *in vivo* fitness and virulence potential during infection (Jimenez et al., 2020; Kumar et al., 2020). We therefore determined whether the attenuation of colitis observed in CR-infected *Mgll* KO mice corresponds with decreased *in vivo* activation of the LEE. CR recovered from cecal contents of *Mgll* KO mice at day 7 post-infection exhibited decreased expression of the LEE-encoded translocon component *espA* and the effector and intimin receptor *tir* compared to CR recovered from *Mgll* WT mice, both of which are essential for disease (Figures 3C and 3D). Notably, the decreased expression of LEE-encoded genes in CR recovered from *Mgll* KO mice precedes the significant reduction in tissue colonization and fecal shedding observed at day 10 (Figures 2A–2E). These data suggest the LEE in CR is not activated to the same extent in *Mgll* KO versus *Mgll* WT mice during infection.

Because colonic 2-AG levels are increased in *Mgll* KO mice, we next assessed whether decreased LEE expression in *Mgll* KO mice may be the result of direct effects of 2-AG on AE pathogen virulence. We performed RNA sequencing (RNA-seq) analysis to investigate whether 2-AG can alter the pathogen transcriptome *in vitro* under well-established LEE inducing growth conditions (Abe et al., 2002; RNA-seq accession number PRJEB29880). RNA-seq was conducted in EHEC grown *in vitro* in the presence of vehicle or of 10 μM 2-AG, which is within the physiological range reported in the human and murine intestines (Alhouayek et al., 2011; Di Sabatino et al., 2011). 2-AG significantly altered the expression of four KEGG pathways, including the bacterial secretion system and pathogenic *E. coli* infection pathways (Figure S4A). Gene-level analyses revealed that these results corresponded with a significant downregulation of numerous LEE-encoded genes including *espA* (Figure S4B). In contrast, few non-LEE-encoded genes were differentially expressed in EHEC in response to 2-AG (RNA-seq accession number PRJEB29880), including the lethal phage-encoded virulence factor Shiga toxin (*stx2a*) (Figure S4C). The inhibitory effects of 2-AG on LEE transcription were confirmed by qRT-PCR of representative LEE-encoded genes from its five operons in EHEC and in *CR* (Figures 3E and S4D). 2-AG did not affect the *in vitro* growth of EHEC or CR (Figures S4E–S4G), suggesting that the inhibitory effects of 2-AG on the LEE are not the result of a decrease in bacterial density. Hence, the host 2-AG inhibits the expression of LEE virulence genes in human and murine AE pathogens.

To functionally confirm the inhibitory effects of 2-AG on the LEE, we next investigated whether 2-AG can inhibit LEE-encoded T3SS activity. In both EHEC and CR, 2-AG significantly reduced EspA and EspB proteins in whole-cell lysates and in the corresponding supernatants (Figures 3F–3I), which together indicates decreased EspA and EspB secretion. Because the biological activity of 2-AG is inactivated through its isomerization to 1-AG (van der Stelt et al., 2002), we next determined whether 1-AG can also inhibit the LEE. In contrast to 2-AG, 1-AG did not inhibit LEE expression (Figures 3J and 3K). Finally, we also tested whether a second ubiquitous endocannabinoid in the gut, arachidonoyl ethanolamide (AEA), which also contains an arachidonic acid moiety, can modulate the LEE. In contrast to 2-AG, anandamide does not inhibit EspA secretion in EHEC (Figure S4H), thus

demonstrating the distinct inhibitory effects of 2-AG on the LEE compared to other endocannabinoids. Collectively, these transcriptional and functional studies demonstrate that 2-AG can act directly on AE pathogens to decrease their pathogenicity by inhibiting an essential virulence factor, thus introducing a mechanism by which CR infection is attenuated in mice with elevated 2-AG.

The Endocannabinoid 2-AG Attenuates T3SS-Dependent Pathogen Interactions with the Host

AE pathogens utilize the LEE-encoded T3SS to form AE lesions on epithelial cells. This process can be observed *in vitro* on epithelial monolayers through the visualization of pedestals—the co-localization of attached pathogens with the polymerization of the epithelial actin cytoskeleton (Figure 4B, white arrow-heads) (Knutton et al., 1989). Inactivation of the LEE in EHEC completely abrogates the formation of these lesions (Elliott et al., 2000). Moreover, the expression and functionality of the LEE correlates with the number of pedestals that are formed per cell, as well as the number of infected cells (Abe et al., 2002; Sircili et al., 2004). This provides a highly controlled experimental system to test the effects of specific host factors on the virulence potential of AE pathogens. We utilized this approach to test whether 2-AG can inhibit EHEC pedestal formation on HeLa cells. To further remove any effects of 2-AG on epithelial cell function, which may impact susceptibility to EHEC infection, we pre-treated EHEC with 2-AG prior to infection with HeLa cells (Figure 4A). 2-AG-conditioned EHEC infected significantly fewer epithelial cells and formed approximately 50% less pedestals compared to untreated EHEC controls (Figures 4B–4D). We next assessed whether manipulation of epithelial 2-AG production can also modulate EHEC pedestal formation. We utilized Caco-2 monolayers that express functional 2-AG biosynthetic enzymes and thus produce 2-AG (Ligresti et al., 2003). Using this system, we investigated whether inhibiting epithelial 2-AG biosynthesis with the diacylglycerol lipase (DAGL) inhibitor tetrahydrolipstatin (THL), which is an FDA-approved weight loss product known as orlistat or Alli, can modulate EHEC pedestal formation. In monolayers that were treated with the DAGL inhibitor, the percentage of epithelial cells infected with EHEC pedestals was significantly increased at 5 and 6 h post-infection (Figures 4E and 4F). These data demonstrate that 2-AG decreases EHEC attachment to epithelial cells and consequent formation of AE lesions that mediate intestinal disease caused by AE pathogens.

Other enteric pathogens such as *S. typhimurium* also utilize T3SS-based strategies to establish successful infection in the gut (Santos et al., 2001). We investigated whether 2-AG can also inhibit T3SS-dependent virulence in *S. typhimurium*. *S. typhimurium* harbors two pathogenicity islands, SPI-1 and SPI-2, that each encode T3SSs that confer epithelial invasiveness and intracellular replication, respectively (Figure 5A; Galán and Curtiss, 1989; Ochman et al., 1996). To determine whether 2-AG can modulate SPI-1 activity, we first cultured *S.* t*yphimurium* under SPI-1-inducing conditions in the presence of 2-AG. qRT-PCR of representative SPI-1 genes revealed that 2-AG inhibited the expression of the SPI-1 master transcriptional regulator *hilD* and the SPI-1 effectors *sipA* and *sopB* (Figures 5B–5D), which corresponded with the decreased secretion of SipA (Figure S5A). When cultured under SPI-2 inducing conditions, the presence of 2-AG also decreased expression of SPI-2

genes including the T3SS apparatus protein *ssaV* and the SPI-2 effector *sseF* (Figures 5E and 5F; Hurley et al., 2014). Importantly, 2-AG did not alter the growth kinetics of *S. typhimurium* (Figure S5B), suggesting that the decreased expression of virulence genes in the presence of 2-AG is not the result of any detrimental effects on *Salmonella* growth.

We next investigated whether 2-AG can also inhibit SPI-1 and SPI-2-dependent virulence functions in *S. typhimurium*. *Mgll* KO mice with elevated 2-AG levels are protected against enteric infection with *S. typhimurium* utilizing the well-established streptomycin model of *Salmonella* infection (Barthel et al., 2003). Streptomycin treatment is necessary for the induction of SPI-1-dependent colon pathology as mice not pretreated with this antibiotic prior to *Salmonella* infection develop Typhoid-like systemic disease (Santos et al., 2001; Barthel et al., 2003). *Mgll* KO mice exhibited modest but statistically significant protection against *S. typhimurium* infection as assessed by survival rates (Figure 5G). However, as expected with antibiotic treatment, fecal abundances of *S. typhimurium* did not differ between *Mgll* WT and KO mice (Figure S5C). We therefore turned to *in vitro Salmonella* infection models to assess the direct effects of 2-AG on SPI-1 and SPI-2-associated virulence functions, epithelial invasion, and intracellular replication, in a more controlled manner. Similar to our observations with EHEC, pretreatment of *S. typhimurium* with 2-AG prior to infection of epithelial monolayers reduced SPI-1-dependent invasion of epithelial cells by approximately 50% (Figure 5H). Moreover, addition of 2-AG to infected epithelial monolayers did not further reduce *Salmonella* invasion, demonstrating that 2-AG pretreatment was sufficient to reduce SPI-1-dependent virulence (Figure 5H). With respect to SPI-2-dependent virulence, the presence of 2-AG also corresponded with decreased intracellular survival of *S. typhimurium* within cultured macrophages (Figure 5I). Hence, in addition to its inhibitory effects on A/E pathogens, 2-AG inhibits T3SS-dependent virulence functions in *S. typhimurium*, therefore demonstrating the broader anti-virulence effects of 2-AG on Enterobacteriaceae enteric pathogens.

2-AG Mediates Its Anti-virulence Effects through Inhibition of the Pro-virulence Bacterial Sensor QseC

Because 2-AG can attenuate the virulence of AE pathogens, we next sought to identify a putative mechanism by which 2-AG exerts its inhibitory effects. The structure of 2-AG is composed of a long-chain fatty acid moiety, arachidonic acid, that is covalently bonded to a glycerol backbone at the *sn2* position (Figure 1A; Mechoulam et al., 1995). In Enterobacteriaceae, including *Salmonella*, *E. coli*, and CR, FadL is the only identified long-chain fatty acid transporter and is localized to the outer membrane (OM) (Dirusso and Black, 2004). Based on the structure of 2-AG, we therefore hypothesized that FadL may also import 2-AG across the OM. To address this, we tested whether 2-AG modulates LEE activity in an isogenic *fadL* mutant (Pifer et al., 2018), reasoning that a lack of LEE inhibition in response to 2-AG would support the involvement of FadL in 2-AG transport. EspA and EspB secretion were no longer attenuated in the *fadL* mutant (Figures 6A and 6B), demonstrating that FadL is necessary for pathogen sensing of 2-AG. We next attempted to investigate how *Mgll* KO mice with elevated 2-AG levels respond to infection with an isogenic *fadL* mutant in *CR*. However, deletion of *fadL* rendered CR unable to stably colonize the murine gut (Figures S6A and S6B).

In several pathogens, including EHEC, CR, and *S. typhimurium*, the host neurotransmitters epi and NE are sensed by the bacterial pro-virulence receptor QseC. QseC activation by epi/NE promotes AE pathogen colonization of the gut through the positive regulation of their LEE-encoded virulence programs and enhanced LEE-encoded T3SS activity (Clarke et al., 2006; Rasko et al., 2008; Curtis et al., 2014). Similarly, epi/NE generally serve as positive signals in mammalian physiology, which are counteracted by the inhibitory effects of endocannabinoids (Szabo and Schlicker, 2005). We therefore hypothesized that 2-AG inhibits QseC-mediated activation of the LEE as its mechanism of action. To test this, we first assessed whether LEE activity is also attenuated in the presence of 2-AG in *qseC* isogenic mutants constructed in EHEC and CR. In contrast to the parental strains, 2-AG failed to inhibit the LEE in the *qseC* mutants as assessed by LEE expression and EspA and EspB secretion (Figures 6C, 6D, S6C, and S6D). Together, these data suggest that QseC may be critical for 2-AG sensing in AE pathogens.

QseC is a HK that autophosphorylates upon activation by epi/NE and then transfers this phosphate to downstream regulators, which initiates complex signaling cascades that ultimately activate the LEE (Njoroge and Sperandio, 2012; Hughes et al., 2009). Therefore, we next investigated whether 2-AG acts through QseC to mediate its anti-virulence effects. To accomplish this, we utilized a reductionist approach where purified QseC was reconstituted into liposomes in the presence of labeled ATP and added 2-AG to assess its effects on QseC activity. QseC activation as assessed by autophosphorylation was significantly diminished in the presence of 2-AG, including with the addition of its agonist epi (Figures 6E and 6F). To further demonstrate that 2-AG engages with QseC, we introduced the endocannabinoid signaling inhibitor AM251, which antagonizes the host endocannabinoid receptor CB1 (Gatley et al., 1996). As reported in mammalian cells, the CB1 antagonist prevented 2-AG inhibition of QseC activity in our *in vitro* liposome system (Figure 6G). Notably, 2-AG did not inhibit the activation of CpxA, a non-adrenergic HK that senses indole and serotonin (Figure S6E) (Kumar and Sperandio, 2019; Kumar et al., 2020), suggesting that 2-AG does not inhibit the activation of other HKs expressed in AE pathogens. 2-AG-mediated inhibition of the LEE is retained in EHEC mutants that lack the non-adrenergic HKs TorS or FusK, the latter of which has also been implicated in regulating the LEE (Figures S6F and S6G; Pacheco et al., 2012). Collectively, these results support a mechanistic model where 2-AG exerts its anti-virulence effects on AE pathogens by crossing the outer membrane through FadL and then engaging with QseC to inhibit subsequent activation of the LEE (Figure 6K).

Because 2-AG seems to exert its anti-virulence effects through the inhibition of the provirulence receptor QseC, we investigated whether this interaction contributes to the protection from *CR* infection observed in *Mgll* KO mice with elevated 2-AG. To test this, we challenged *Mgll* WT and KO mice with CR WT or the *qseC* mutant that is unable to sense 2-AG. As we have previously reported, CR colonization of the gut is attenuated in mice infected with the *qseC* mutant (Figures 6H and 6I). In contrast to *Mgll* KO mice colonized with the parental CR strain, where pathogen burdens are decreased in feces and in cecal tissues with increased host 2-AG, we observed similar fecal and cecal burdens of the *qseC* mutant in *Mgll* KO mice compared to *Mgll* WT mice (Figures 6H and 6I). Notably, the percentage of mice with cecal tissues positive for the *qseC* mutant by culture were

comparable between *Mgll* WT and KO mice infected with the *qseC* mutant (both at 62.5%) (Figure 6I). While this infection rate is lower than *Mgll* WT mice colonized with the parental CR strain (94.4%), the rate of infection remained most attenuated in *Mgll* KO mice infected with the parental CR strain (28.9%) (Figure 6I). Similar trends were observed with fecal pathogen shedding (Figure 6H). Moreover, the severity of disease as assessed by gross pathology did not differ between *Mgll* WT and KO mice colonized with the *qseC* mutant and was not as attenuated as in *Mgll* KO mice colonized with the 2-AG responsive parental strain (Figure 6J). Finally, because 2-AG can impact host neurotransmitter activity and epi/NE exert direct pro-virulence effects on AE pathogens, we assessed whether colonic NE levels differed between *Mgll* WT and KO mice as an alternative explanation for the decreased *CR* virulence in *Mgll* KO mice. We observed that colonic NE was comparable between *Mgll* WT and KO mice (Figure S6H), thus further supporting our hypothesis that 2-AG attenuates intestinal infection through its anti-virulence effects. Collectively, our findings suggest that 2-AG directly attenuates the virulence potential of AE pathogens by inhibiting the activation of QseC, which contributes to the protection against enteric infection by AE pathogens observed in mice with elevated 2-AG. More broadly, our findings establish that host endocannabinoids directly modulate bacterial function, which in turn can impact host-bacterial interactions and the outcomes of GI disease.

DISCUSSION

Anecdotal evidence linked the use of cannabis and other phytocannabinoids such as cannabidiol (CBD) with alleviating symptoms associated with various GI disorders including inflammatory bowel diseases and irritable bowel syndrome (Goyal et al., 2017; Perisetti et al., 2020). This lead to discovery of the role of the endocannabinoid system (ECS) in regulating GI physiology, immunity, and susceptibility to disease (Turcotte et al., 2015; Leinwand et al., 2017b; Taschler et al., 2017; Hasenoehrl et al., 2016). Genetic or pharmacological inactivation of host ECS generally exerts anti-inflammatory effects in numerous animal models of inflammatory disease (Turcotte et al., 2015), including experimental models of intestinal inflammation, such as chemically induced and non-infectious models (Massa et al., 2004; Engel et al., 2008, 2010; Romano et al., 2013; Shamran et al., 2017; D'Argenio et al., 2006; Andrzejak et al., 2011; Storr et al., 2008; Zhao et al., 2017; El Bakali et al., 2014; Leinwand et al., 2017a; Alhouayek et al., 2011), which primarily delineated host-centric mechanisms that explain how endocannabinoids mediate their anti-inflammatory effects. The GI microbiota has also been implicated in endocannabinoid modulation of host physiology and disease (Cani et al., 2016). Microbiota membership correlate with altered endocannabinoid tone, while abrogation of endocannabinoid signaling is associated with changes to the microbiota (Geurts et al., 2011; Everard et al., 2013; Guida et al., 2018, 2020; Manca et al., 2020; Mehrpouya-Bahrami et al., 2017). We built upon this to (1) establish that the ECS also impacts host susceptibility to infection and (2) to introduce and define a bacterial-mediated mechanism that contributes to the anti-inflammatory effects of endocannabinoids. We show that mice with increased levels of the endocannabinoid 2-AG are less susceptible to the AE pathogen CR. 2-AG antagonizes the pro-virulence bacterial receptor QseC, inhibiting virulence-associated T3SS functions in mouse and human AE pathogens that are essential for intestinal colonization and disease.

Finally, this protection against CR infection is attenuated when pathogen sensing of host 2-AG by QseC is disrupted. Taken together, we introduce a defined host-pathogen molecular interaction by which endocannabinoids impart their anti-inflammatory effects in addition to their established effects on the host.

Genetic ablation and pharmacological blockade of Mgll leads to accumulation of 2-AG in colon tissues (Figure 1B; Nomura et al., 2011; Taschler et al., 2015). Mice with elevated 2-AG are less susceptible to CR infection (Figures 1 and 2). Specifically, increased levels of 2-AG in the host promotes earlier pathogen clearance while minimally impacting its initial establishment. This effect is more pronounced in female *Mgll* KO mice, which interestingly exhibit a trend toward increased colonic 2-AG compared to males. The sexual dimorphic characteristics of the mammalian ECS has been well established in the brain and reproductive system (Craft et al., 2013; Bradshaw et al., 2006; Wagner, 2016). To our knowledge, the observation of sexual dimorphism with ECS manipulations in the context of experimental colitis has not been previously reported. Pharmacological blockade of *Mgll* prior to CR infection recapitulates this phenotype, suggesting that any changes in endocannabinoid or immune tone as a result of lifelong *Mgll* deficiency unlikely contributes to this effect. From the 11 immune markers investigated in colon and cecum tissues of WT and KO mice, the levels of only three were altered. However, we acknowledge that the small changes in the basal expression of these few immune markers (*Lcn2*, *Il10*, and *Il12b*) in the colons of *Mgll* KO mice (Figures S2E and S2F) may also contribute to modulating the host response to enteric infection. Future experiments aiming to address this are granted. In both *Mgll* KO mice and mice subjected to pharmacological blockade of Mgll, decreased intestinal colonization at days 7 and 10 correspond with minimal activation of proinflammatory host responses, such as the nuclear factor κB (NF-κB)-regulated gene *Nos2* compared to uninfected controls, and attenuated histopathology and pathology. This suggests that the increased CR clearance in mice with elevated 2-AG is not the result of an accelerated infectious life cycle as activation of immune responses and tissue pathology would likely be evident at day 7 as CR is cleared from cecal tissues. Moreover, decreased expression of the LEE in CR in *Mgll* KO mice precedes the biggest differences in fecal and cecal CR colonization between WT and KO mice observed at day 10. Hence, our findings support a model where decreased LEE expression corresponds with reduced intestinal pathology and faster CR clearance in mice with elevated 2-AG.

The extent of LEE expression correlates with the ability of AE pathogens to cause disease (Figures 1, 2, and 3). CR mutants unable to sense LEE-activating signals are attenuated. However, several of these mutants are not completely avirulent and unable to colonize the gut (Curtis et al., 2014b; Moreira et al., 2016; Pifer et al., 2018; Menezes-Garcia et al., 2020). The Δ*qseC* can still colonize mice, albeit to a lesser degree than WT CR. The virulence dampening effects of 2-AG observed when KO mice are infected with WT CR are not observed when these animals are infected with Δ*qseC* (Figures 6H–6J). Finally, antagonizing host sensing of 2-AG through CB2 did not restore disease severity in mice subjected to chronic Mgll inhibition (Figures 2G–2J). We note that the CB2 inhibitor inhibits the host, but not the bacterial, response to 2-AG, further suggesting that 2-AG also attenuates infection by dampening the virulence potential of the pathogen.

Pathogens encounter a complex intestinal chemistry (Kumar et al., 2019). They engage with these signals to gauge the appropriate location and infection timing to deploy virulence programs that maximize their colonization of the gut. AE pathogens sense 2-AG through its inhibition of QseC decreasing LEE expression, gut colonization, and disease. The levels of 2-AG are higher in the small intestine compared to the colon (DiPatrizio et al., 2015). EHEC and CR both colonize the cecum and colon in a LEE-dependent manner (Kaper et al., 2004). Thus, it is tempting to speculate that 2-AG could be a host factor that prohibits the permissiveness of infection by these pathogens in the small intestine. 2-AG levels are regulated by the activities of Mgll and the 2-AG biosynthetic enzymes, which are expressed apically at the epithelium (Marquéz et al., 2009). To our knowledge, the 2-AG biosynthesis by microbes has not been reported. Thus, 2-AG concentrations are likely highest at the mucosal interface, where the LEE-encoded T3SS is deployed to facilitate pathogen attachment and AE lesion formation. Since mice with elevated 2-AG exhibit faster clearance of infection, it is also possible that 2-AG may serve as a signal for pathogens to initiate their exit strategy to infect the next host. Future studies to investigate the role of 2-AG in infection resolution and pathogen transmission are needed. Thus, one can speculate that in mice with elevated 2-AG, the inhibitory effects of 2-AG override the provirulence effects of NE (Moreira et al., 2016), thus promoting faster tissue clearance of CR. Together, the interplay between NE and 2-AG may serve as local signals for AE pathogens to tightly regulate their virulence-associated T3SSs to successful complete their infectious life cycle. Future studies should define how host NE and 2-AG concentrations fluctuate along the GI tract during infection and impact pathogen-mediated gut colonization and disease.

Finally, our findings also introduce the potential for broader effects of 2-AG in modulating bacterial function. 2-AG also inhibits T3SS-dependent functions in *Salmonella* including epithelial invasion and intramacrophage survival and lead to a modest increase in survival in *Mgll* KO mice subjected to the streptomycin model of *Salmonella* gastroenteritis. However, it should be noted that given the lethality of this model, it is difficult to observe faster clearance of intestinal infection that we observed with CR, the latter of which represents a natural infection model. QseC regulates the expression of SPI-1 and SPI-2 genes (Bearson and Bearson, 2008; Moreira et al., 2010; Moreira and Sperandio, 2012; Li et al., 2016); hence, it is likely that 2-AG exerts its effects in *Salmonella* through QseC. Moreover, because QseC regulates virulence in other pathogens (Rasko et al., 2008; Kostakioti et al., 2009; Hadjifrangiskou et al., 2011; Curtis et al., 2014a; Halang et al., 2015), it will be interesting to investigate whether 2-AG also inhibits their virulence, particularly in extraintestinal sites of infection. Finally, QseC expression is not restricted to pathogens and is encoded within the core genomes of commensal bacteria. QseC activation by epi/NE regulates other bacterial behaviors such as flagellar motility and contributes to the intestinal fitness and proinflammatory potential of commensal *E. coli* associated with inflammatory bowel diseases (Sperandio et al., 2002; Rooks et al., 2017). Thus, 2-AG may also modulate additional aspects of bacterial function that affect host-commensal interactions and host susceptibility to disease. Modulation of host immune function by 2-AG may be especially important during opportunistic infections by non-professional pathogens, and future studies are necessary to delve into the complexity of these interactions. Taken together, our findings

introduce a defined host-pathogen molecular interaction by which endocannabinoids dampen virulence of enteric pathogens in addition to their established effects on the host.

STAR★METHODS

RESOURCE AVAILABILITY

Lead Contact—Further information and request for resources and reagents should be directed to and will be fulfilled by the Lead Contact, Vanessa Sperandio (vanessa.sperandio@utsouthwestern.edu).

Materials Availability—Bacteria mutant strains are available by request made to the lead contact.

Data and Code Availability—RNA-Seq data can be accessed using the accession number PRJEB29880 at the European Nucleotide Archive at https://www.ebi.ac.uk/ena/browser/home.

16*S* rRNA microbiota profiling data can be accessed using the accession number SubmissionID: SUB8062197 BioProject ID: PRJNA660086 at the NCBI SRA database.

EXPERIMENTAL MODEL AND SUBJECT DETAILS

Mice—*Mgll*$^{+/-}$ breeding pairs were recovered from cryopreservation (Texas A&M Institute for Genomic Medicine) and utilized to generate a mouse colony at UT Southwestern. Genotypes were confirmed using the following primer pairs: Mgll 5′ F7: GGAAACAGGTTTGT CATGGC, Mgll 3′ R1: GCGAGAAACCAGAAGGAGAC. C57BL/6 WT mice were purchased from The Jackson Laboratory. All mice were group housed in specific pathogen free conditions at UT Southwestern and maintained on a 12 hr light/dark cycle with unlimited access to water and food (Telkad Global 16% Protein Rodent Diet, Envigo). Unless otherwise indicated, male and female mice at 8–12 weeks of age were utilized for *in vivo* infections or mock infections with phosphate buffered saline (PBS). For all experiments, female littermates were randomly assigned by genotype to experimental groups. Male littermates of the same genotype were maintained in the same experimental groups, as randomization led to fighting and lethal wounds. All animal protocols were approved by the UT Southwestern Medical Center Institutional Animal Care and Use Committee.

Epithelial Cells—HeLa cells and Caco-2 cells were obtained from the ATCC and stored in liquid nitrogen until used. Cells were maintained in Dulbecco eagle medium (DMEM) medium with 4.5 g/L glucose and supplemented with 10% fetal bovine serum (FBS) and 1% penicillin/streptomycin/gentamicin antibiotic mix at 37°C, 5% CO_2.

Murine Macrophages—J774.1 murine macrophages were obtained from the ATCC and stored in liquid nitrogen until used. Cells were maintained in DMEM medium with 4.5 g/L glucose and supplemented with 10% FBS and 1% PSG at 37°C, 5% CO_2.

Bacterial Strains—Enterohemorrhagic *Escherichia coli* (EHEC) strain 86–24, *Citrobacter rodentium* strain DBS100, and *Salmonella enterica* serovar Typhimurium strains IR715 and SL1344 were grown overnight in Luria bertani (LB) broth at 250 rpm and 37°C prior to subculture for *in vitro* experiments or mouse infections as described below. Antibiotics were added as appropriate for maintenance of plasmids. All bacteria at stationary phase was mixed with sterile glycerol (25% final concentration) and kept as stocks at −80°C.

METHOD DETAILS

Strains, Plasmids and Growth Conditions—Bacterial strains and plasmids used in this study are listed in Table S1. The isogenic mutants utilized in this study and their respective citations are listed in Table S1 and were generated using the lambda red recombinase method (Datsenko and Wanner, 2000) (Baba et al., 2006). EHEC and *CR* were subcultured into established LEE-inducing conditions as follows: DMEM medium with 1 g/L glucose and grown as standing cultures (microaerobic) or shaking at 250 rpm (aerobic) at 37°C (Abe et al., 2002) (Njoroge et al., 2012) (Carlson-Banning and Sperandio, 2016). *S.* Typhimurium strains were subcultured into LB broth for SPI-1-inducing conditions or subcultured into N9 minimal medium for SPI-2-inducing conditions and grown aerobically at 250 rpm at 37°C (Galán and Curtiss, 1989) (Lee et al., 2000) (Deiwick et al., 1999). Where indicated, bacteria were grown in the presence of 2-arachidonoyl glycerol, 2-AG (Tocris), 1-arachidonoyl glycerol, 1-AG (Cayman Chemical), anandamide (Tocris) or the vehicle control (methanol at a final concentration of 1:10000).

CR Infections With Mgll−/− Mice—At 8–12 weeks of age, male and female *Mgll*+/− or *Mgll*−/− mice, or *Mgll*+/+ littermate controls, were orally gavaged with 1×10^9 CFU of *CR* DBS100 or mock infected with PBS in a 100 μL volume. Fecal pellets were collected throughout the course of infection to enumerate fecal pathogen loads by quantitative culture using selective media with nalidixic acid. Feces were weighed, resuspended in PBS, and homogenized prior to plating. At necropsy, colon tissues were harvested to quantify *CR* burden, for pathology analysis, for lipid analysis and for RNA isolation. Colon contents were collected for quantitative bacterial culture, bacterial RNA isolation, 16S rRNA profiling or norepinephrine quantification. All experiments were performed with at least two independent cohorts and sample sizes are indicated in the figure legends.

CR Infections With Inhibitors—Eight to 12-week-old female *Mgll*−/− mice and *Mgll* +/+ littermate controls, or C57BL/6 mice purchased from Jackson Laboratory, were utilized for these experiments. Where indicated, mice were chronically administered the Mgll inhibitor JZL184 (Cayman Chemical) by I.P. at 16 mg/kg, once every 24 hours for 5 days, prior to the start of infection (Long et al., 2009) (Schlosburg et al., 2010). Where indicated, mice were administered the cannabinoid receptor 2 inhibitor AM630 (Cayman Chemical) by I.P. at 10 mg/kg, once every 24 hours for 5 days, prior to the start of infection. Mice were administered AM630 or vehicle control approximately 30 minutes prior to receiving JZL184 or vehicle control. The last dose was administered on the same day of infection, approximately 30 minutes prior to gavage with *CR*. All pharmacological agents were dissolved in DMSO with gentle heating as needed and mixed with Tween-80 and PBS as a vehicle at a final ratio of 18:1:1 (PBS/Tween-80/DMSO). Following these treatments, mice

were gavaged with 1×10^9 CFU of *CR* DBS100 or mock infected with PBS. Fecal pellets were collected throughout the course of infection to enumerate fecal pathogen loads by quantitative culture using selective media with nalidixic acid. At necropsy, colon tissues were harvested to quantify *CR* burden and for pathology analysis. Colon contents were collected for quantitative bacterial culture. All experiments were performed with at least two independent cohorts with the exception of the group co-administered JZL184 and AM630 (1 cohort). Sample sizes are indicated in the figure legends.

Fecal Microbiota Transplantations (FMT)—Germ free (GF) C57BL/6 mice were maintained in gnotobiotic isolators at UT Southwestern. One cohort of GF female mice at 8–12 weeks of age (n = 6) served as FMT recipients. Eight to 12-week-old female *Mgll*−/− mice and *Mgll*+/+ littermate controls served as FMT donors. Fecal pellets were freshly collected from a cage of 4 mice and were mixed in PBS (approximately 1 pellet/200 μL volume). Fecal samples were centrifuged to remove debris. FMT recipients were gavaged with 100 μL of the prepared fecal mixtures under sterile conditions and were maintained under gnotobiotic housing. Seven days following FMT, mice were gavaged with 1×10^9 CFU of *CR* DBS100 to initiate infection. At necropsy, following seven days of infection, colon tissues were harvested to quantify *CR* burden and for pathology analysis. Colon contents were collected for quantitative bacterial culture.

Gross Pathology And Histopathology—At necropsy, colitis severity was first grossly assessed, including colon lengths and qualitative assessment of cecal atrophy (0–4), thickening of cecal (0–5) and colon tissues (0–4), extent of content loss in the cecum (0–4) and diarrhea (0–3). Total gross pathology scores are based on a scale from 0–20. For histopathology assessment, the cecal tip and distal colon segments were washed in PBS and fixed in 10% neutral buffered formalin. The tissues were embedded in paraffin, cut into 5-mm sections, and stained with hematoxylin and eosin (H&E) in the UT Southwestern Pathology Core. Histological inflammation scores of H&E stained colon sections were blindly assessed as previously described (Gibson et al., 2008). Briefly, inflammation was assessed based on the following histopathological features: submucosal edema (0–4), goblet cell depletion (0–4), epithelial hyperplasia (0–4), epithelial integrity (0–4), and polymononuclear (PMN) cell and inflammatory monocyte infiltration (0–4). In the distal colon, the presence and severity of crypt abscesses (0–3) was also assessed. Data are expressed as the sum of these individual scores (0–20 for cecum, 0–23 for distal colon).

S. enterica Infections—At 8–12 weeks of age, male and female WT or *Mgll*$^{-/-}$ mice on the C57BL/6 background were intragastrically administered 20 mg of streptomycin as previously described (*19*). After 24 hours, mice were orally infected with 1×10^9 CFU of *S. enterica* Typhimurium IR715 WT or the SPI-1-deficient mutant, Δ*invA*. Fecal pellets were collected throughout the course of infection to enumerate fecal pathogen loads by quantitative culture using selective media with nalidixic acid. Severity of disease was assessed by mouse survival. All experiments were performed with at least two independent cohorts. Sample sizes are indicated in the figure legends.

RNA Isolation And Quantitative Real-Time PCR—RNA was isolated from cecal tissues snap frozen in liquid nitrogen using the TriZol method (Thermo Fisher Scientific) according to the manufacturer's instructions. For *CR* expression of LEE genes *in vivo*, RNA was isolated from cecal contents snap frozen in liquid nitrogen using the RNeasy PowerMicrobiome Kit (QIAGEN) according to the manufacturer's instructions. For *in vitro* bacterial RNA isolations, all strains were grown to mid-log or late-log phase as indicated, pelleted, harvested in TriZol reagent and bacterial RNA was subsequently extracted using the RiboPure bacterial isolation kit (Ambion) per the manufacturer's instructions. cDNA was synthesized using SuperScript II reverse transcriptase (ThermoFisher Scientific). qRT-PCR was performed in a QuantStudio 6 Flex Instrument (Life Technologies) with Power SYBR Green (Applied Biosystems) using the following PCR conditions: a single hold at 50°C for 2 minutes and at 95°C for 10 minutes, followed by 40 cycles at 95°C for 15 s and 60°C for 1 minute. Each PCR was performed in 10 μL reactions and contained the following: 1x SYBR green mix and 0.25 μM of each primer. Melting curves were assessed to ensure specificity of the PCR products. Data were collected using QuantStudio real-time PCR software v1.3. The relative abundance of mammalian mRNA transcripts was calculated using the delta delta CT method and normalized to *Gapdh* levels. The relative abundance of bacterial mRNA transcripts was calculated using the delta delta CT method and normalized to *rpoA* levels. All *in vitro* assays were repeated in at least three independent experiments. The oligonucleotides used in this study for qRT-PCR are listed in Table S2.

Western Blot For Secreted Proteins—Secreted proteins were isolated at the indicated time points following centrifugation of samples as previously described (Jarvis et al., 1995). Bovine serum albumin (BSA) was used as a loading control and added to secreted protein samples. Cell pellets were resuspended in 8M urea to harvest lysate-associated proteins. Proteins were separated by a gradient 4%–15% SDS-PAGE gel, transferred to a polyvinylidene fluoride membrane and blocked with 5% milk or 5% BSA in PBS with 0.05% Tween-20. Membranes were probed with anti-EspA, anti-EspB or anti-Tir primary antibodies, followed by incubation with secondary antibodies conjugated to streptavidin-horseradish peroxidase. Membranes were exposed using the Bio-Rad ChemiDoc™ Touch Imaging System (Software 1.0.0.15) with Image Lab 5.2.1 software for image analysis and densitometry. All secretion assays were repeated in at least three independent experiments.

Fluorescent Actin Staining (FAS) Assay—FAS assays were performed on HeLa cells or Caco-2 cells as previously described (Knutton et al., 1989). Briefly, epithelial cells were grown to 80%–90% confluency on coverslips in DMEM medium with 4.5 g/L glucose and supplemented with 10% FBS and 1% penicillin/streptomycin. Three hours prior to infection, HeLa cells were incubated in DMEM medium with 1 g/L glucose and without serum and antibiotics. Prior to infection, mCherry-expressing EHEC was subcultured in DMEM with 0.1% glucose to mid-log phase in the presence of 2-AG or the vehicle control. Epithelial cells were then infected at a MOI of 1–10, which was confirmed by quantitative plating. Where indicated, 30-min prior to infection with EHEC, Caco-2 cells were treated with the inhibitor tetrahydrolipstatin at 10 μM or vehicle control (methanol, final concentration 1:2000). At the indicated time points, the samples were washed, fixed, permeabilized and stained with fluorescein Isothiocyanate (FITC)-labeled phalloidin to visualize actin and

4′,6-diamidino-2-phenylindole (DAPI) to visualize DNA. The coverslips were then mounted on slides and images for pedestal enumeration were taken using the Zeiss LSM780 confocal/multiphoton microscope at the UT Southwestern Live Cell Imaging Core Facility. Pedestal formation was quantified in two ways - as the number of pedestals per infected cell and the percentage of epithelial cells that contain pedestals. Replicate coverslips from at least two independent experiments were quantified.

Epithelial Invasion Assay—*S.* Typhimurium epithelial invasion assays were performed on HeLa cells as previously described (Finlay et al., 1991). Briefly, HeLa cells were grown to 80%–90% confluency in DMEM medium with 4.5 g/L glucose and supplemented with 10% FBS and 1% penicillin/streptomycin. Three hours prior to infection, HeLa cells were incubated in DMEM medium with 1 g/L glucose and without serum and antibiotics (infection medium). Prior to infection, *S.* Typhimurium strain SL1344 was cultured in LB medium until OD_{600} = 1.0 in the presence of 2-AG or the vehicle control. Epithelial cells were then infected at a MOI of 10 for 1 hour, followed by PBS washes and incubation with gentamicin in infection medium for 1 hour to remove extracellular bacteria. Epithelial cells were lysed with 1% Triton X-100 and intracellular bacteria were enumerated by quantitative bacterial culture. All invasion assays were repeated in three independent experiments.

Macrophage Infections—*S.* Typhimurium macrophage infections were performed as previously described (Moreira et al., 2010). Briefly, J774.1 murine macrophages were infected with opsonized *S.* Typhimurium SL1344 at an MOI of 100 for 30 minutes, followed by treatment with 40 μg/ml of gentamicin for 1 hour to kill extracellular bacteria. Macrophages were lysed with 1% Triton X-100 to release intracellular bacteria for enumeration by quantitative bacterial culture. Where indicated, 6 μM of 2-AG and/or the cannabinoid receptor 1 inhibitor AM251 were added to overnight cultures and at the start of infection. All macrophage infections were repeated in three independent experiments.

CpxA And QseC Purification—The histidine kinases CpxA and QseC were purified as previously described (Clarke et al., 2006) (Kumar and Sperandio, 2019). Briefly, *E. coli* (BL21 DE3) harboring pET21a-CpxA (His-tagged) or pVS155 (pBAD-QseC-MycHis) were grown until stationary phase (OD_{600} ~0.7–0.8). Cultures were induced with 0.1 mM IPTG or arabinose and incubated overnight at 18°C. The bacterial cultures were spun down at 10,000 rpm, 4°C for 30 minutes and the pellets were stored at −80°C until further use. The bacterial pellets were resuspended in lysis buffer (50 mM Tris pH 8.0, 150 mM NaCl, 2% lauryldimethylamine N-oxide (LDAO), 10% glycerol) and protease inhibitor cocktail was added. The lysates were sonicated for 30 s ON and 30 s OFF for 8 minutes at 85% amplitude, followed by centrifugation at 10,000 rpm, 4°C for 30 minutes. The supernatants were filtered using 0.22 μm filter tubes. Then, 500 μl of Ni-NTA beads were added to 40 mL of lysate and incubated on a shaker for up to 2 hours at 4°C to allow protein binding to the Ni-beads. The bound lysates were then passed through 5 mL disposable columns twice. The column was washed with 5 column volumes of wash buffer (50 mM Tris pH 8.0, 150 mM NaCl, 30 mM Imidazole). Proteins were then eluted from the column with elution buffer (50 mM Tris pH8.0, 150 mM NaCl, 250 mM Imidazole). The eluted proteins were concentrated down using Amicon Ultra 15 Centrifugal Filter Units (10 kDa) and excess imidazole was

removed by adding dialyzing buffer (50 mM Tris pH 8.0 and 150 mM NaCl). Protein concentrations were estimated using the Bradford assay and were immediately loaded onto liposomes for autophosphorylation assays.

Autophosphorylation Assays—Autophosphorylation assays were performed as previously described (Clarke et al., 2006). Liposomes were reconstituted with CpxA or QseC as described (Clarke et al., 2006) (Kumar and Sperandio, 2019). Briefly, 50 mg of *E. coli* phospholipids (20 mg/mL in chloroform) were evaporated and then dissolved into 5 mL phosphate buffer containing 80 mg N-octyl-β-D-glucopyranoside. The solution was dialyzed overnight against phosphate buffer. The resulting liposome suspension underwent freeze/thaw cycles in liquid N_2. The liposomes were stored at −80°C until further use. The liposomes (1 mL) were destabilized by the addition of 5.8 mg dodecylmaltoside, followed by addition of CpxA-His or QseC-His at a ratio of 40:1 and stirring at room temperature for 10 minutes. Then 58 mg of Biobeads were added to remove the detergent and the resulting solution was allowed to incubate at 4°C overnight. The supernatant was then incubated with fresh Biobeads (58 mg) for 1 hour. The resulting liposomes containing the reconstituted His-tagged proteins were used for autophosphorylation experiments. The initiate the autophosphorylation assay, 10 μL of the liposomes reconstituted with the His-tagged protein were adjusted to 10 mM MgCl2 and 1 mM DTT, and then, one of the following signals was added: 10 μM 2-AG, 50 μM epinephrine,10 μM of the cannabinoid receptor 1 antagonist AM251, 8 μM arachidonic acid, 500 μM indole, or the vehicle control. The resulting mixtures were then rapidly frozen in liquid N2 and thawed, followed by incubation at room temperature for 1 hour and then addition of 0.25 μL [γ32P] ATP to each reaction. At each time point, 2 μL of 5X SDS loading buffer was added to stop the reactions. The samples were then run on 12% SDS-PAGE according to standard procedures and visualized using a phosphoimager (Typhoon FLA 9500, GE).

RNaseq Preparation And Analysis—RNA isolated from four biological replicates was used for RNaseq analysis. Samples were sequenced at the UT Southwestern Medical Center Genomics and Microarray Core. RNA libraries were prepared using Illumina ScriptSeq Complete Kit for bacteria. RNA libraries were run on the Illumina HiSeq 2500 sequencer with SE-50. To analyze the data, reads were trimmed, decontaminated and quality-filtered using BBmap software suite. Reads were mapped to the *Escherichia coli* O157:H7 str. EDL933 genome using Bowtie2. Number of reads of each gene was determined using the featureCounts package and differential expression was analyzed using DESeq2. The accession number for the data is PRJEB29880 at the European Nucleotide Archive.

16S rRNA Sequencing And Analysis—Genomic DNA was isolated from feces collected from female *Mgll* WT or KO littermates at ages 5 and 8 weeks of age (n = 4 per group) for 16S rRNA microbiota profiling. The hypervariable region V3 & V4 of bacterial 16*S* rRNA gene were captured using the Illumina Nextera protocol. A single amplicon of about 460 bp was amplified using the 16*S* Forward Primer 5′TCGTCGGCAGCGTC AGATGTGTATAAGAGACAGCCTACGGGNGGCWGCAG and the 16*S* Reverse Primer 5′GTCTCGTGGGCTCGGAGATGTGTAT AAGAGACAGGACTACHVGGGTATCTAATCC as described in the Illumina protocol. The

PCR product were cleaned using Agencourt AmpureXP beads from Beckman Counter Genomics. Illumina adaptor and barcode sequences were ligated to the amplicons in order to attach them to MiSeqDx flow cell and for multiplexing. Quality and quantity of each sequencing library was assessed using Bioanlyzer and picogreen measurements, respectively. About 6 pM of pooled libraries was loaded onto a MiSeqDX flow cell and sequenced using PE300 (Paired end 300 bp) v3 kit. Raw fastq files were demultiplexed based on unique barcodes and assessed for quality. Samples with more than 50 K QC pass sequencing reads were used for downstream 16*S* operational taxonomic units (OTU) analysis. The accession number for the raw fastq files is pending at the NCBI SRA database.

16S Analysis Pipeline—Taxonomic classification and OTU abundance analysis was done using CLC Bio microbial genomics module (https://digitalinsights.qiagen.com/plugins/clc-microbial-genomics-module/). Individual sample reads were annotated with the Greengene database and taxonomic features were determined. Alpha and beta diversity analysis was done to understand the within and between sample diversity, respectively. Abundance data was used for numeric Principal Component Analysis (PCA) in SVS, Golden Helix Software.

Lipid Extraction From Colon Tissues—Distal colon samples were collected for lipid analysis from PBS mock-infected or *CR* infected (3 days post infection) male and female *Mgll* WT, HET or KO littermates at 8–12 weeks of age. Sample sizes are indicated in the figure legends. All solvents utilized for lipid analysis were either HPLC or LC/MS grade and purchased from Sigma-Aldrich. All lipid extractions were performed in 16 × 100 mm glass tubes with PTFE-lined caps (Fisher Scientific, Pittsburg, PA, USA). Glass Pasteur pipettes and solvent-resistant plasticware pipette tips (Mettler-Toledo) were used to minimize leaching of polymers and plasticizers. Approximately 100 mg of tissue was weighed and added to 1 mL of methanol/dichloromethane (1:2, v/v) in a 2.0-mL pre-filled Bead Ruptor tube (2.8 mm ceramic beads, Omni International). Tissue was homogenized with a Bead Ruptor (Omni International) for 50 s (5.5 mps, 3 cycles, 10 s/cycle, 5 s dwell time). The homogenates were transferred to glass tubes and diluted to a final concentration of 20 mg/mL using methanol/dichloromethane (1:2, v/v).

Fatty Acid Profiling By GC-MS—Fatty acid profiles were generated by a modified GC-MS method previously described by (Quehenberger et al., 2011). Briefly, 0.5 mg of tissue homogenate was transferred to a glass tube where 1 mL of MeOH with 50 mM HCl, 1 mL of water, 1 mL of iso-octane, and 100 μL of 0.5 μg/mL of FA(20:4 ω6{$^{2}H_{8}$}) fatty acid standard in methanol were added. The mixture was vortexed for 5 minutes in a tube shaker and centrifuged at 2671 × *g* for an additional 5 minutes. The organic phase was collected to a fresh glass tube. The procedure was repeated two times and the organic phases collected were pooled together and dried under N_2. Dried lipid extract was resuspended in 50 μL of 1% triethylamine in acetone, and derivatized with 50 μL of 1% pentafluorobenzyl bromide (PFBBr) in acetone at room temperature for 25 minutes in capped glass tubes. Solvents were dried under N_2, and samples were resuspended in 500 μL of isooctane. Samples were analyzed using an Agilent 7890/5975C (Santa Clara, CA, USA) by electron capture negative ionization (ECNI) equipped with a DB-5MS column (40 m ч 0.180 mm with 0.18 μm film thickness) from Agilent. Hydrogen (carrier gas) flow rate was 1.6 mL/min and injection port

temperature was set at 300°C. Sample injection volume was 1 μL. Initial oven temperature was set at 150°C, and then increased to 200°C at a 25°C/min, followed by an increase of 8°C/minute until a temperature of 300°C was reached and held for 2.2 minutes, for a total run time was 16.7 minutes. Fatty acids were analyzed in selected ion monotoring (SIM) mode. The FA data was normalized to the internal standard. Data was processed using MassHunter software (Agilent).

LC-MS/MS Analysis Of Monoacylglycerols—Aliquots equivalent to 0.5 mg of homogenized tissue were transferred to fresh glass tubes for liquid-liquid extraction (LLE). The samples were dried under N_2 and extracted by Bligh/Dyer (Bligh and Dyer, 1959); 1 mL each of chloroform, methanol, and water were added to a glass tube containing the sample. The mixture was vortexed and centrifuged at 2671 × *g* for 5 minutes, resulting in two distinct liquid phases. The organic phase was collected to a fresh glass tube with a Pasteur pipette and dried under N_2. Samples were resuspended in Hexane. The monoacylglycerols were analyzed by LC-MS/MS using a SCIEX QTRAP 6500^+ equipped with a Shimadzu LC-30AD (Kyoto, Japan) HPLC system and a 150 × 2.1 mm, 5 μm Supelco Ascentis silica column (Bellefonte, PA, USA). Samples were injected at a flow rate of 0.3 mL/min at 2.5% solvent B (methyl tert-butyl ether) and 97.5% Solvent A (Hexane). Solvent B is increased to 5% during 3 minutes and then to 60% over 6 minutes. Solvent B is decreased to 0% during 30 s while Solvent C (90:10 (v/v) isopropanol-water) is set up at 20% and increased to 40% during the following 11 minutes. Solvent C is increased to 50% during 6 minutes. The system was held at 50% of solvent C during 5 minutes prior to re-equilibration at 2.5% of solvent B for 15 minutes. Solvent D (95:5 (v/v) acetonitrile-water with 10 mM ammonium acetate) was infused post-column at 0.03mL/min. Column oven temperature was set to 25°C. Data was acquired in positive mode in positive ion mode using multiple reaction monitoring (MRM) of the *m/z* transitions 379.3→287.3, 331.3→239.2, 359.3→264.2, 357.3→265.2, 355.3→263.2, 387.2→295.2, 383.3→291.2, 381,3→289.2 and 403.4→311.2. The LC-MS data was analyzed using MultiQuant software (SCIEX). Electrospray ionization source parameters were, GS1 40, Cur 20, temperature 150°C, declustering potential 60, and collision energy 25. GS1 and 2 were zero-grade air while Cur and CAD gas was nitrogen.

Norepinephrine Measurements In Feces—Cecal contents were collected from 8–12-week old *Mgll* WT or KO mice at sacrifice. The samples were then frozen immediately at −80°C and subjected to processing as described (Wojnicz et al., 2016). Briefly, the samples were homogenized for protein precipitation in an ice-cold solution containing 75% acetonitrile, 1% formic acid and 0.2 μM of the internal standard (DL-Norepinephrine hydrochloride) in a 4:1 proportion (solvent:cecum content). The samples were then centrifugated at high speed (~17000 *g*) for 40 minutes at 4°C. 200 μL of the supernatant were collected, evaporated to dryness at 45°C, resuspended in 100 μL of mobile phase (95:5, 0.2%formic acid:acetonitrile) and injected directly into the LC-MS-MS apparatus (Triple Quad 6500, Sciex) for analysis.

QUANTIFICATION AND STATISTICAL ANALYSIS

The statistical tests, definition of center, dispersion and precision measures and sample sizes are indicated within each figure legend. Generally, *P*-values were calculated using Student's t test when 2 experimental groups were compared and one-way ANOVA with Bonferroni multiple comparison post test when 3 or more experimental groups were compared. All enumeration of bacteria by serial dilution and plating was log transformed to normalize the data. For microscopy, histology and pathology analyses, *p-value*s were calculated using Mann-Whitney when 2 experimental groups were compared and Kruskal-Wallis test with the Dunn's post test when 3 or more experimental groups were compared. Statistics for survival analysis was calculated using the log rank (Mantel-Cox) test. For all experiments with mice, the collected data was subject to normality tests (Anderson-Darling, D'Agostino, Shapiro-Wilk and Kolmogorov-Smirnov)to determine the appropriate use of parametric or non-parametric statistical tests. A *p-value* of < 0.05 was considered statistically significant. All statistical tests were performed using Prism 8 version 8.4.2 (GraphPad Software, LLC). Statistical significance was defined as follows: * $p < 0.05$, ** $p < 0.01$, *** $p < 0.001$, **** $p < 0.0001$.

Supplementary Material

Refer to Web version on PubMed Central for supplementary material.

ACKNOWLEDGMENTS

We thank Michael Brown and David Russell at UTSW for reviewing this manuscript. We thank Lora Hooper at UTSW for help with the germ-free experiments and reviewing this manuscript. We acknowledge the Texas A&M Institute for Genomic Medicine for the *Mgll*$^{+/-}$ breeding pairs, the UTSW Live Cell Imaging Core for confocal microscopy, the UTSW Histopathology Core for assisting with sample preparation, the UTSW Genomics and Microarray Core for RNA-seq library preparation and sequencing, the UTSW Microbiome Research Laboratory for 16S rRNA sequencing services and analysis, and Raechel Chanin for experimental help. This study was supported by the NIH grants AI053067, AI05135, AI077613, and AI114511 to V.S. A.G.J. was supported through NIH training grant 5 T32 AI7520–14.

REFERENCES

Abe H, Tatsuno I, Tobe T, Okutani A, and Sasakawa C (2002). Bicarbonate ion stimulates the expression of locus of enterocyte effacement-encoded genes in enterohemorrhagic Escherichia coli O157:H7. Infect. Immun 70, 3500–3509. [PubMed: 12065489]

Alhouayek M, Lambert DM, Delzenne NM, Cani PD, and Muccioli GG (2011). Increasing endogenous 2-arachidonoylglycerol levels counteracts colitis and related systemic inflammation. FASEB J 25, 2711–2721. [PubMed: 21551239]

Andrzejak V, Muccioli GG, Body-Malapel M, El Bakali J, Djouina M, Renault N, Chavatte P, Desreumaux P, Lambert DM, and Millet R (2011). New FAAH inhibitors based on 3-carboxamido-5-aryl-isoxazole scaffold that protect against experimental colitis. Bioorg. Med. Chem 19, 3777–3786. [PubMed: 21612933]

Baba T, Ara T, Hasegawa M, Takai Y, Okumura Y, Baba M, Datsenko KA, Tomita M, Wanner BL, and Mori H (2006). Construction of Escherichia coli K-12 in-frame, single-gene knockout mutants: the Keio collection. Mol. Syst. Biol 2, 2006.0008.

Barthel M, Hapfelmeier S, Quintanilla-Martínez L, Kremer M, Rohde M, Hogardt M, Pfeffer K, Rüssmann H, and Hardt W-D (2003). Pretreatment of mice with streptomycin provides a Salmonella enterica serovar Typhimurium colitis model that allows analysis of both pathogen and host. Infect. Immun 71, 2839–2858. [PubMed: 12704158]

Bäumler AJ, and Sperandio V (2016). Interactions between the microbiota and pathogenic bacteria in the gut. Nature 535, 85–93. [PubMed: 27383983]

Bearson BL, and Bearson SMD (2008). The role of the QseC quorumsensing sensor kinase in colonization and norepinephrine-enhanced motility of Salmonella enterica serovar Typhimurium. Microb. Pathog 44, 271–278. [PubMed: 17997077]

Bisogno T, Sepe N, Melck D, Maurelli S, De Petrocellis L, and Di Marzo V (1997). Biosynthesis, release and degradation of the novel endogenous cannabimimetic metabolite 2-arachidonoylglycerol in mouse neuroblastoma cells. Biochem. J 322, 671–677. [PubMed: 9065792]

Blankman JL, Simon GM, and Cravatt BF (2007). A comprehensive profile of brain enzymes that hydrolyze the endocannabinoid 2-arachidonoylglycerol. Chem. Biol 14, 1347–1356. [PubMed: 18096503]

Bligh EG, and Dyer WJ (1959). A rapid method of total lipid extraction and purification. Can. J. Biochem. Physiol 37, 911–917. [PubMed: 13671378]

Bradshaw HB, Rimmerman N, Krey JF, and Walker JM (2006). Sex and hormonal cycle differences in rat brain levels of pain-related cannabimimetic lipid mediators. Am. J. Physiol. Regul. Integr. Comp. Physiol 291, R349–R358. [PubMed: 16556899]

Cani PD, Plovier H, Van Hul M, Geurts L, Delzenne NM, Druart C, and Everard A (2016). Endocannabinoids–at the crossroads between the gut microbiota and host metabolism. Nat. Rev. Endocrinol 12, 133–143. [PubMed: 26678807]

Carlson-Banning KM, and Sperandio V (2016). Catabolite and Oxygen Regulation of Enterohemorrhagic Escherichia coli Virulence. MBio 7, e01852–e16. [PubMed: 27879335]

Clarke MB, and Sperandio V (2005). Transcriptional regulation of flhDC by QseBC and sigma (FliA) in enterohaemorrhagic Escherichia coli. Mol. Microbiol 57, 1734–1749. [PubMed: 16135237]

Clarke MB, Hughes DT, Zhu C, Boedeker EC, and Sperandio V (2006). The QseC sensor kinase: a bacterial adrenergic receptor. Proc. Natl. Acad. Sci. USA 103, 10420–10425. [PubMed: 16803956]

Côtes K, Dhouib R, Douchet I, Chahinian H, de Caro A, Carrière F, and Canaan S (2007). Characterization of an exported monoglyceride lipase from Mycobacterium tuberculosis possibly involved in the metabolism of host cell membrane lipids. Biochem. J 408, 417–427. [PubMed: 17784850]

Craft RM, Marusich JA, and Wiley JL (2013). Sex differences in cannabinoid pharmacology: a reflection of differences in the endocannabinoid system? Life Sci 92, 476–481. [PubMed: 22728714]

Curtis MM, Russell R, Moreira CG, Adebesin AM, Wang C, Williams NS, Taussig R, Stewart D, Zimmern P, Lu B, et al. (2014a). QseC inhibitors as an antivirulence approach for Gram-negative pathogens. MBio 5, e02165–e14. [PubMed: 25389178]

Curtis MM, Hu Z, Klimko C, Narayanan S, Deberardinis R, and Sperandio V (2014b). The gut commensal Bacteroides thetaiotaomicron exacerbates enteric infection through modification of the metabolic landscape. Cell Host Microbe 16, 759–769. [PubMed: 25498343]

D'Argenio G, Valenti M, Scaglione G, Cosenza V, Sorrentini I, and Di Marzo V (2006). Up-regulation of anandamide levels as an endogenous mechanism and a pharmacological strategy to limit colon inflammation. FASEB J 20, 568–570. [PubMed: 16403786]

Datsenko KA, and Wanner BL (2000). One-step inactivation of chromosomal genes in Escherichia coli K-12 using PCR products. Proc. Natl. Acad. Sci. USA 97, 6640–6645. [PubMed: 10829079]

Deiwick J, Nikolaus T, Erdogan S, and Hensel M (1999). Environmental regulation of Salmonella pathogenicity island 2 gene expression. Mol. Microbiol 31, 1759–1773. [PubMed: 10209748]

Deng W, Puente JL, Gruenheid S, Li Y, Vallance BA, Vázquez A, Barba J, Ibarra JA, O'Donnell P, Metalnikov P, et al. (2004). Dissecting virulence: systematic and functional analyses of a pathogenicity island. Proc. Natl. Acad. Sci. USA 101, 3597–3602. [PubMed: 14988506]

Deutsch DG, and Chin SA (1993). Enzymatic synthesis and degradation of anandamide, a cannabinoid receptor agonist. Biochem. Pharmacol 46, 791–796. [PubMed: 8373432]

Devane WA, Hanus L, Breuer A, Pertwee RG, Stevenson LA, Griffin G, Gibson D, Mandelbaum A, Etinger A, and Mechoulam R (1992). Isolation and structure of a brain constituent that binds to the cannabinoid receptor. Science 258, 1946–1949. [PubMed: 1470919]

Dhouib R, Laval F, Carrière F, Daffé M, and Canaan S (2010). A monoacylglycerol lipase from Mycobacterium smegmatis Involved in bacterial cell interaction. J. Bacteriol 192, 4776–4785. [PubMed: 20601476]

Di Sabatino A, Battista N, Biancheri P, Rapino C, Rovedatti L, Astarita G, Vanoli A, Dainese E, Guerci M, Piomelli D, et al. (2011). The endogenous cannabinoid system in the gut of patients with inflammatory bowel disease. Mucosal Immunol 4, 574–583. [PubMed: 21471961]

Dinh TP, Carpenter D, Leslie FM, Freund TF, Katona I, Sensi SL, Kathuria S, and Piomelli D (2002). Brain monoglyceride lipase participating in endocannabinoid inactivation. Proc. Natl. Acad. Sci. USA 99, 10819–10824. [PubMed: 12136125]

Dinh TP, Kathuria S, and Piomelli D (2004). RNA interference suggests a primary role for monoacylglycerol lipase in the degradation of the endocannabinoid 2-arachidonoylglycerol. Mol. Pharmacol 66, 1260–1264. [PubMed: 15272052]

DiPatrizio NV, Igarashi M, Narayanaswami V, Murray C, Gancayco J, Russell A, Jung K-M, and Piomelli D (2015). Fasting stimulates 2-AG biosynthesis in the small intestine: role of cholinergic pathways. Am. J. Physiol. Regul. Integr. Comp. Physiol 309, R805–R813. [PubMed: 26290104]

Dirusso CC, and Black PN (2004). Bacterial long chain fatty acid transport: gateway to a fatty acid-responsive signaling system. J. Biol. Chem 279, 49563–49566. [PubMed: 15347640]

El Bakali J, Muccioli GG, Body-Malapel M, Djouina M, Klupsch F, Ghinet A, Barczyk A, Renault N, Chavatte P, Desreumaux P, et al. (2014). Conformational Restriction Leading to a Selective CB2 Cannabinoid Receptor Agonist Orally Active Against Colitis. ACS Med. Chem. Lett 6, 198–203. [PubMed: 25699149]

Elliott SJ, Sperandio V, Girón JA, Shin S, Mellies JL, Wainwright L, Hutcheson SW, McDaniel TK, and Kaper JB (2000). The locus of enterocyte effacement (LEE)-encoded regulator controls expression of both LEE- and non-LEE-encoded virulence factors in enteropathogenic and enterohemorrhagic Escherichia coli. Infect. Immun 68, 6115–6126. [PubMed: 11035714]

Engel MA, Kellermann CA, Rau T, Burnat G, Hahn EG, and Konturek PC (2008). Ulcerative colitis in AKR mice is attenuated by intraperitoneally administered anandamide. J. Physiol. Pharmacol 59, 673–689. [PubMed: 19212003]

Engel MA, Kellermann CA, Burnat G, Hahn EG, Rau T, and Konturek PC (2010). Mice lacking cannabinoid CB1-, CB2-receptors or both receptors show increased susceptibility to trinitrobenzene sulfonic acid (TNBS)-induced colitis. J. Physiol. Pharmacol 61, 89–97. [PubMed: 20228420]

Everard A, Belzer C, Geurts L, Ouwerkerk JP, Druart C, Bindels LB, Guiot Y, Derrien M, Muccioli GG, Delzenne NM, et al. (2013). Crosstalk between Akkermansia muciniphila and intestinal epithelium controls diet-induced obesity. Proc. Natl. Acad. Sci. USA 110, 9066–9071. [PubMed: 23671105]

Finlay BB, Ruschkowski S, and Dedhar S (1991). Cytoskeletal rearrangements accompanying salmonella entry into epithelial cells. J. Cell Sci 99, 283–296. [PubMed: 1909337]

Galán JE, and Curtiss R 3rd. (1989). Cloning and molecular characterization of genes whose products allow Salmonella typhimurium to penetrate tissue culture cells. Proc. Natl. Acad. Sci. USA 86, 6383–6387. [PubMed: 2548211]

Gatley SJ, Gifford AN, Volkow ND, Lan R, and Makriyannis A (1996). 123I-labeled AM251: a radioiodinated ligand which binds in vivo to mouse brain cannabinoid CB1 receptors. Eur. J. Pharmacol 307, 331–338. [PubMed: 8836622]

Geurts L, Lazarevic V, Derrien M, Everard A, Van Roye M, Knauf C, Valet P, Girard M, Muccioli GG, François P, et al. (2011). Altered gut microbiota and endocannabinoid system tone in obese and diabetic leptin-resistant mice: impact on apelin regulation in adipose tissue. Front. Microbiol 2, 149. [PubMed: 21808634]

Gibson DL, Ma C, Rosenberger CM, Bergstrom KSB, Valdez Y, Huang JT, Khan MA, and Vallance BA (2008). Toll-like receptor 2 plays a critical role in maintaining mucosal integrity during Citrobacter rodentium-induced colitis. Cell. Microbiol 10, 388–403. [PubMed: 17910742]

Goyal H, Singla U, Gupta U, and May E (2017). Role of cannabis in digestive disorders. Eur. J. Gastroenterol. Hepatol 29, 135–143. [PubMed: 27792038]

Guida F, Turco F, Iannotta M, De Gregorio D, Palumbo I, Sarnelli G, Furiano A, Napolitano F, Boccella S, Luongo L, et al. (2018). Antibiotic-induced microbiota perturbation causes gut endocannabinoidome changes, hippocampal neuroglial reorganization and depression in mice. Brain Behav. Immun 67, 230–245. [PubMed: 28890155]

Guida F, Boccella S, Belardo C, Iannotta M, Piscitelli F, De Filippis F, Paino S, Ricciardi F, Siniscalco D, Marabese I, et al. (2020). Altered gut microbiota and endocannabinoid system tone in vitamin D deficiency-mediated chronic pain. Brain Behav. Immun 85, 128–141. [PubMed: 30953765]

Hadjifrangiskou M, Kostakioti M, Chen SL, Henderson JP, Greene SE, and Hultgren SJ (2011). A central metabolic circuit controlled by QseC in pathogenic Escherichia coli. Mol. Microbiol 80, 1516–1529. [PubMed: 21542868]

Halang P, Toulouse C, Geißel B, Michel B, Flauger B, Müller M, Voegele RT, Stefanski V, and Steuber J (2015). Response of Vibrio cholerae to the Catecholamine Hormones Epinephrine and Norepinephrine. J. Bacteriol 197, 3769–3778. [PubMed: 26416829]

Hapfelmeier S, Ehrbar K, Stecher B, Barthel M, Kremer M, and Hardt W-D (2004). Role of the Salmonella pathogenicity island 1 effector proteins SipA, SopB, SopE, and SopE2 in Salmonella enterica subspecies 1 serovar Typhimurium colitis in streptomycin-pretreated mice. Infect. Immun 72, 795–809. [PubMed: 14742523]

Hasenoehrl C, Taschler U, Storr M, and Schicho R (2016). The gastrointestinal tract - a central organ of cannabinoid signaling in health and disease. Neurogastroenterol. Motil 28, 1765–1780. [PubMed: 27561826]

Hughes DT, Clarke MB, Yamamoto K, Rasko DA, and Sperandio V (2009). The QseC adrenergic signaling cascade in Enterohemorrhagic E. coli (EHEC). PLoS Pathog 5, e1000553. [PubMed: 19696934]

Hurley D, McCusker MP, Fanning S, and Martins M (2014). Salmonella-host interactions - modulation of the host innate immune system. Front. Immunol 5, 481. [PubMed: 25339955]

Jarvis KG, Girón JA, Jerse AE, McDaniel TK, Donnenberg MS, and Kaper JB (1995). Enteropathogenic Escherichia coli contains a putative type III secretion system necessary for the export of proteins involved in attaching and effacing lesion formation. Proc. Natl. Acad. Sci. USA 92, 7996–8000. [PubMed: 7644527]

Jimenez AG, Ellermann M, Abbott W, and Sperandio V (2020). Dietderived galacturonic acid regulates virulence and intestinal colonization in enterohaemorrhagic Escherichia coli and Citrobacter rodentium. Nat. Microbiol 5, 368–378. [PubMed: 31873206]

Kaper JB, Nataro JP, and Mobley HL (2004). Pathogenic Escherichia coli. Nat. Rev. Microbiol 2, 123–140. [PubMed: 15040260]

Knutton S, Baldwin T, Williams PH, and McNeish AS (1989). Actin accumulation at sites of bacterial adhesion to tissue culture cells: basis of a new diagnostic test for enteropathogenic and enterohemorrhagic Escherichia coli. Infect. Immun 57, 1290–1298. [PubMed: 2647635]

Kostakioti M, Hadjifrangiskou M, Pinkner JS, and Hultgren SJ (2009). QseC-mediated dephosphorylation of QseB is required for expression of genes associated with virulence in uropathogenic Escherichia coli. Mol. Microbiol 73, 1020–1031. [PubMed: 19703104]

Kumar A, and Sperandio V (2019). Indole Signaling at the Host-Microbiota-Pathogen Interface. MBio 10, e01031–e19. [PubMed: 31164470]

Kumar A, Ellermann M, and Sperandio V (2019). Taming the Beast: Interplay between Gut Small Molecules and Enteric Pathogens. Infect. Immun 87, 87.

Kumar A, Russell RM, Pifer R, Menezes-Garcia Z, Cuesta S, Narayanan S, MacMillan JB, and Sperandio V (2020). The Serotonin Neurotransmitter Modulates Virulence of Enteric Pathogens. Cell Host Microbe 28, 41–53. [PubMed: 32521224]

Lee AK, Detweiler CS, and Falkow S (2000). OmpR regulates the two-component system SsrA-ssrB in Salmonella pathogenicity island 2. J. Bacteriol 182, 771–781. [PubMed: 10633113]

Leinwand KL, Jones AA, Huang RH, Jedlicka P, Kao DJ, de Zoeten F, Ghosh S, Moaddel R, Wehkamp J, Ostaff MJ, et al. (2017a). Cannabinoid Receptor-2 Ameliorates Inflammation in Murine Model of Crohn's Disease. J. Crohn's Colitis 11, 1369–1380. [PubMed: 28981653]

Leinwand KL, Gerich ME, Hoffenberg EJ, and Collins CB (2017b). Manipulation of the Endocannabinoid System in Colitis: A Comprehensive Review. Inflamm. Bowel Dis 23, 192–199. [PubMed: 28079617]

Li Z, Zheng Q, Xue X, Shi X, Zhou Y, Da F, Qu D, Hou Z, and Luo X (2016). Pyroptosis of Salmonella Typhimurium-infected macrophages was suppressed and elimination of intracellular bacteria from macrophages was promoted by blocking QseC. Sci. Rep 6, 37447. [PubMed: 27853287]

Ligresti A, Bisogno T, Matias I, De Petrocellis L, Cascio MG, Cosenza V, D'argenio G, Scaglione G, Bifulco M, Sorrentini I, and Di Marzo V (2003). Possible endocannabinoid control of colorectal cancer growth. Gastroenterology 125, 677–687. [PubMed: 12949714]

Long JZ, Li W, Booker L, Burston JJ, Kinsey SG, Schlosburg JE, Pavón FJ, Serrano AM, Selley DE, Parsons LH, et al. (2009). Selective blockade of 2-arachidonoylglycerol hydrolysis produces cannabinoid behavioral effects. Nat. Chem. Biol 5, 37–44. [PubMed: 19029917]

Luperchio SA, and Schauer DB (2001). Molecular pathogenesis of Citrobacter rodentium and transmissible murine colonic hyperplasia. Microbes Infect 3, 333–340. [PubMed: 11334751]

Manca C, Boubertakh B, Leblanc N, Deschˆ nes T, Lacroix S, Martin C, Houde A, Veilleux A, Flamand N, Muccioli GG, et al. (2020). Germ-free mice exhibit profound gut microbiota-dependent alterations of intestinal endocannabinoidome signaling. J. Lipid Res 61, 70–85. [PubMed: 31690638]

Marquéz L, Suárez J, Iglesias M, Bermudez-Silva FJ, Rodríguez de Fonseca F, and Andreu M (2009). Ulcerative colitis induces changes on the expression of the endocannabinoid system in the human colonic tissue. PLoS ONE 4, e6893. [PubMed: 19730730]

Massa F, Marsicano G, Hermann H, Cannich A, Monory K, Cravatt BF, Ferri G-L, Sibaev A, Storr M, and Lutz B (2004). The endogenous cannabinoid system protects against colonic inflammation. J. Clin. Invest 113, 1202–1209. [PubMed: 15085199]

Mechoulam R, Ben-Shabat S, Hanus L, Ligumsky M, Kaminski NE, Schatz AR, Gopher A, Almog S, Martin BR, Compton DR, et al. (1995). Identification of an endogenous 2-monoglyceride, present in canine gut, that binds to cannabinoid receptors. Biochem. Pharmacol 50, 83–90. [PubMed: 7605349]

Mehrpouya-Bahrami P, Chitrala KN, Ganewatta MS, Tang C, Murphy EA, Enos RT, Velazquez KT, McCellan J, Nagarkatti M, and Nagarkatti P (2017). Blockade of CB1 cannabinoid receptor alters gut microbiota and attenuates inflammation and diet-induced obesity. Sci. Rep 7, 15645. [PubMed: 29142285]

Menezes-Garcia Z, Kumar A, Zhu W, Winter SE, and Sperandio V (2020). l-Arginine sensing regulates virulence gene expression and disease progression in enteric pathogens. Proc. Natl. Acad. Sci. USA 117, 12387–12393. [PubMed: 32409599]

Moreira CG, and Sperandio V (2012). Interplay between the QseC and QseE bacterial adrenergic sensor kinases in Salmonella enterica serovar Typhimurium pathogenesis. Infect. Immun 80, 4344–4353. [PubMed: 23027532]

Moreira CG, Weinshenker D, and Sperandio V (2010). QseC mediates Salmonella enterica serovar typhimurium virulence in vitro and in vivo. Infect. Immun 78, 914–926. [PubMed: 20028809]

Moreira CG, Russell R, Mishra AA, Narayanan S, Ritchie JM, Waldor MK, Curtis MM, Winter SE, Weinshenker D, and Sperandio V (2016). Bacterial Adrenergic Sensors Regulate Virulence of Enteric Pathogens in the Gut. MBio 7, e00826–e16. [PubMed: 27273829]

Mullineaux-Sanders C, Sanchez-Garrido J, Hopkins EGD, Shenoy AR, Barry R, and Frankel G (2019). Citrobacter rodentium-host-microbiota interactions: immunity, bioenergetics and metabolism. Nat. Rev. Microbiol 17, 701–715. [PubMed: 31541196]

Njoroge J, and Sperandio V (2012). Enterohemorrhagic Escherichia coli virulence regulation by two bacterial adrenergic kinases, QseC and QseE. Infect. Immun 80, 688–703. [PubMed: 22144490]

Njoroge JW, Nguyen Y, Curtis MM, Moreira CG, and Sperandio V (2012). Virulence meets metabolism: Cra and KdpE gene regulation in enterohemorrhagic Escherichia coli. MBio 3, e00280–e12. [PubMed: 23073764]

Nomura DK, Hudak CSS, Ward AM, Burston JJ, Issa RS, Fisher KJ, Abood ME, Wiley JL, Lichtman AH, and Casida JE (2008). Monoacylglycerol lipase regulates 2-arachidonoylglycerol action and arachidonic acid levels. Bioorg. Med. Chem. Lett 18, 5875–5878. [PubMed: 18752948]

Nomura DK, Long JZ, Niessen S, Hoover HS, Ng S-W, and Cravatt BF (2010). Monoacylglycerol lipase regulates a fatty acid network that promotes cancer pathogenesis. Cell 140, 49–61. [PubMed: 20079333]

Nomura DK, Morrison BE, Blankman JL, Long JZ, Kinsey SG, Marcondes MCG, Ward AM, Hahn YK, Lichtman AH, Conti B, and Cravatt BF (2011). Endocannabinoid hydrolysis generates brain prostaglandins that promote neuroinflammation. Science 334, 809–813. [PubMed: 22021672]

Ochman H, Soncini FC, Solomon F, and Groisman EA (1996). Identification of a pathogenicity island required for Salmonella survival in host cells. Proc. Natl. Acad. Sci. USA 93, 7800–7804. [PubMed: 8755556]

Pacheco AR, Curtis MM, Ritchie JM, Munera D, Waldor MK, Moreira CG, and Sperandio V (2012). Fucose sensing regulates bacterial intestinal colonization. Nature 492, 113–117. [PubMed: 23160491]

Perisetti A, Rimu AH, Khan SA, Bansal P, and Goyal H (2020). Role of cannabis in inflammatory bowel diseases. Ann. Gastroenterol 33, 134–144. [PubMed: 32127734]

Pifer R, Russell RM, Kumar A, Curtis MM, and Sperandio V (2018). Redox, amino acid, and fatty acid metabolism intersect with bacterial virulence in the gut. Proc. Natl. Acad. Sci. USA 115, E10712–E10719. [PubMed: 30348782]

Quehenberger O, Armando AM, and Dennis EA (2011). High sensitivity quantitative lipidomics analysis of fatty acids in biological samples by gas chromatography–mass spectrometry. Biochim. Biophys. Acta 1811, 648–656. [PubMed: 21787881]

Rasko DA, Moreira CG, Li R, Reading NC, Ritchie JM, Waldor MK, Williams N, Taussig R, Wei S, Roth M, et al. (2008). Targeting QseC signaling and virulence for antibiotic development. Science 321, 1078–1080. [PubMed: 18719281]

Romano B, Borrelli F, Fasolino I, Capasso R, Piscitelli F, Cascio M, Pertwee R, Coppola D, Vassallo L, Orlando P, et al. (2013). The cannabinoid TRPA1 agonist cannabichromene inhibits nitric oxide production in macrophages and ameliorates murine colitis. Br. J. Pharmacol 169, 213–229. [PubMed: 23373571]

Rooks MG, Veiga P, Reeves AZ, Lavoie S, Yasuda K, Asano Y, Yoshihara K, Michaud M, Wardwell-Scott L, Gallini CA, et al. (2017). QseC inhibition as an antivirulence approach for colitis-associated bacteria. Proc. Natl. Acad. Sci. USA 114, 142–147. [PubMed: 27980034]

Santos RL, Zhang S, Tsolis RM, Kingsley RA, Adams LG, and Bäumler AJ (2001). Animal models of Salmonella infections: enteritis versus typhoid fever. Microbes Infect 3, 1335–1344. [PubMed: 11755423]

Sartor RB, and Wu GD (2017). Roles for Intestinal Bacteria, Viruses, and Fungi in Pathogenesis of Inflammatory Bowel Diseases and Therapeutic Approaches. Gastroenterology 152, 327–339. [PubMed: 27769810]

Schlosburg JE, Blankman JL, Long JZ, Nomura DK, Pan B, Kinsey SG, Nguyen PT, Ramesh D, Booker L, Burston JJ, et al. (2010). Chronic monoacylglycerol lipase blockade causes functional antagonism of the endocannabinoid system. Nat. Neurosci 13, 1113–1119. [PubMed: 20729846]

Shamran H, Singh NP, Zumbrun EE, Murphy A, Taub DD, Mishra MK, Price RL, Chatterjee S, Nagarkatti M, Nagarkatti PS, and Singh UP (2017). Fatty acid amide hydrolase (FAAH) blockade ameliorates experimental colitis by altering microRNA expression and suppressing inflammation. Brain Behav. Immun 59, 10–20. [PubMed: 27327245]

Sircili MP, Walters M, Trabulsi LR, and Sperandio V (2004). Modulation of enteropathogenic Escherichia coli virulence by quorum sensing. Infect. Immun 72, 2329–2337. [PubMed: 15039358]

Sperandio V, Torres AG, and Kaper JB (2002). Quorum sensing Escherichia coli regulators B and C (QseBC): a novel two-component regulatory system involved in the regulation of flagella and motility by quorum sensing in E. coli. Mol. Microbiol 43, 809–821. [PubMed: 11929534]

Storr MA, Keenan CM, Emmerdinger D, Zhang H, Yüce B, Sibaev A, Massa F, Buckley NE, Lutz B, Göke B, et al. (2008). Targeting endocannabinoid degradation protects against experimental colitis

in mice: involvement of CB1 and CB2 receptors. J. Mol. Med. (Berl.) 86, 925–936. [PubMed: 18493729]

Szabo B, and Schlicker E (2005). Effects of cannabinoids on neurotransmission. Handb. Exp. Pharmacol 168, 327–365.

Taschler U, Eichmann TO, Radner FPW, Grabner GF, Wolinski H, Storr M, Lass A, Schicho R, and Zimmermann R (2015). Monoglyceride lipase deficiency causes desensitization of intestinal cannabinoid receptor type 1 and increased colonic μ-opioid receptor sensitivity. Br. J. Pharmacol 172, 4419–4429. [PubMed: 26075589]

Taschler U, Hasenoehrl C, Storr M, and Schicho R (2017). Cannabinoid Receptors in Regulating the GI Tract: Experimental Evidence and Therapeutic Relevance. Handb. Exp. Pharmacol 239, 343–362. [PubMed: 28161834]

Turcotte C, Chouinard F, Lefebvre JS, and Flamand N (2015). Regulation of inflammation by cannabinoids, the endocannabinoids 2-arachidonoyl-glycerol and arachidonoyl-ethanolamide, and their metabolites. J. Leukoc. Biol 97, 1049–1070. [PubMed: 25877930]

Turcotte C, Blanchet M-R, Laviolette M, and Flamand N (2016). The CB2 receptor and its role as a regulator of inflammation. Cell. Mol. Life Sci 73, 4449–4470. [PubMed: 27402121]

van der Stelt M, van Kuik JA, Bari M, van Zadelhoff G, Leeflang BR, Veldink GA, Finazzi-Agrò A, Vliegenthart JFG, and Maccarrone M (2002). Oxygenated metabolites of anandamide and 2-arachidonoylglycerol: conformational analysis and interaction with cannabinoid receptors, membrane transporter, and fatty acid amide hydrolase. J. Med. Chem 45, 3709–3720. [PubMed: 12166944]

Wagner EJ (2016). Sex differences in cannabinoid-regulated biology: A focus on energy homeostasis. Front. Neuroendocrinol 40, 101–109. [PubMed: 26800649]

Wojnicz A, Avendaño Ortiz J, Casas AI, Freitas AE, G López M, and Ruiz-Nuño A (2016). Simultaneous determination of 8 neurotransmitters and their metabolite levels in rat brain using liquid chromatography in tandem with mass spectrometry: Application to the murine Nrf2 model of depression. Clin. Chim. Acta 453, 174–181. [PubMed: 26712273]

Zhao X, Liang P, Liu J, Jiang H, Fan X, Chen G, and Zhou C (2017). Elevation of arachidonoylethanolamide levels by activation of the endocannabinoid system protects against colitis and ameliorates remote organ lesions in mice. Exp. Ther. Med 14, 5664–5670. [PubMed: 29285108]

Highlights

- Endocannabinoids such as 2-AG are host lipid hormones that modulate gut biology
- Mice with increased 2-AG are protected from enteric bacterial infection
- 2-AG inhibits virulence programs in EHEC and *C. rodentium* essential for infection
- 2-AG antagonizes the bacterial pro-virulence receptor QseC to decrease virulence

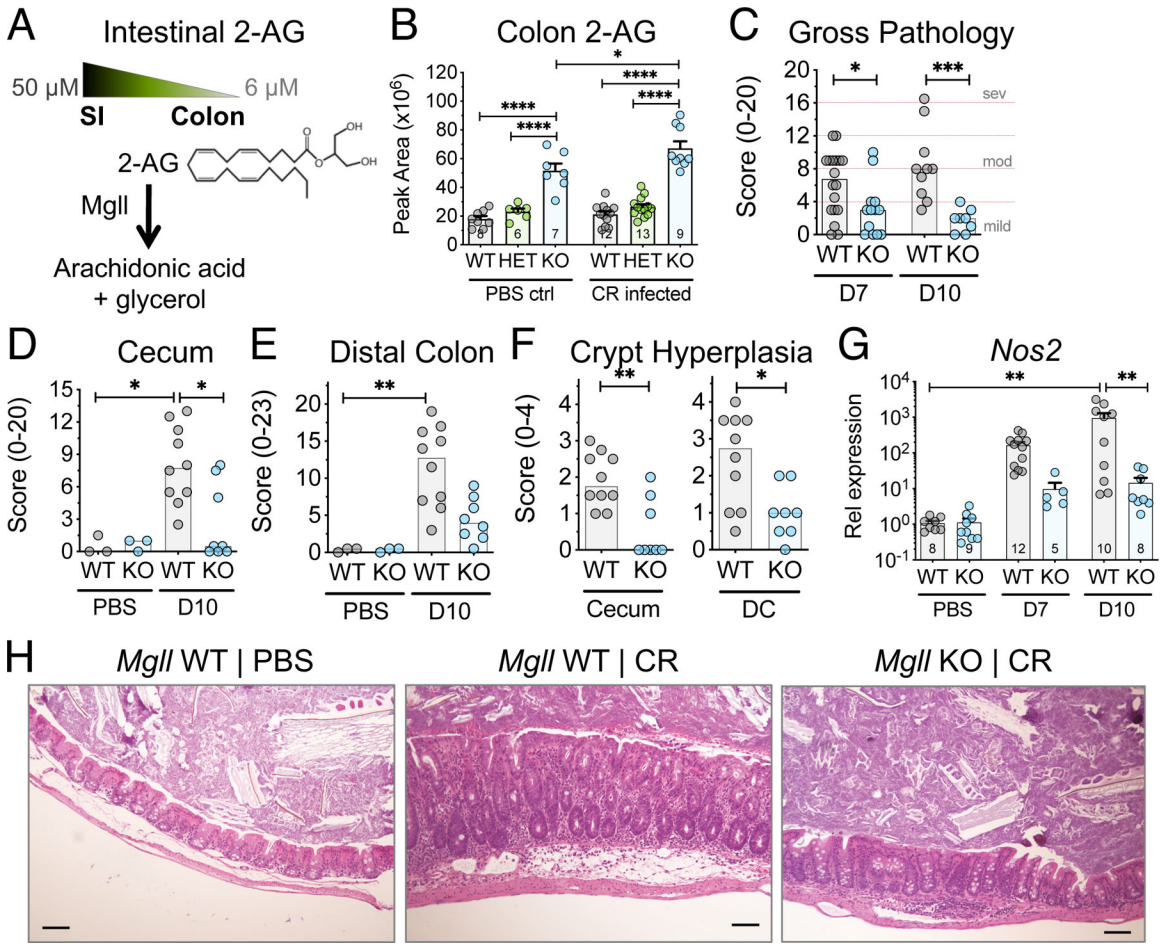

Figure 1. Infectious Disease Induced by *C. rodentium* Is Attenuated in Mice with Elevated 2-Arachidonyl Glycerol Levels

(A) Schematics of 2-arachidonoyl glycerol (2-AG) structure, hydrolysis in mammalian tissues, and gradients in the intestines. SI, small intestines; Mgll, monoacylglycerol lipase.

(B) Quantification of 2-AG in colon tissues harvested from *Mgll* WT, HET, or KO mice gavaged with PBS (mock infected, n = 6–8) or infected with CR (CR, n = 9–13). Data are represented as the mean ± SEM.

(C) Combined gross pathology scores of ceca and colons harvested from CR-infected *Mgll* WT or KO mice at days 7 or 10 post-infection (n = 14–18 for day 7, 8–10 for day 10).

(D and E) Histopathology scores of (D) ceca and (E) colons from PBS-treated (n = 3) or CR-infected (n = 8–10) *Mgll* WT or KO mice at day 10 post-infection.

(F) Hyperplasia scores of ceca and distal colons (DC) from CR-infected *Mgll* WT or KO mice (n = 8–10) at day 10 post-infection. Data in (C)–(F) are represented as the median.

(G) Relative cecal transcript levels of *Nos2* in PBS-treated (n = 8–9) or CR-infected (n = 8–10) *Mgll* WT or KO mice at days 7 or 10 post-infection. Data are represented as the mean ± SEM.

(H) Representative H&E histology of ceca from PBS-treated or CR-infected *Mgll* WT or KO mice at day 10 post-infection. Scale bar, 100 μm.

p values were determined by two-way ANOVA (B), Kruskal-Wallis (D and E), Mann-Whitney (C and F), or one-way ANOVA (G). See also Figure S1.

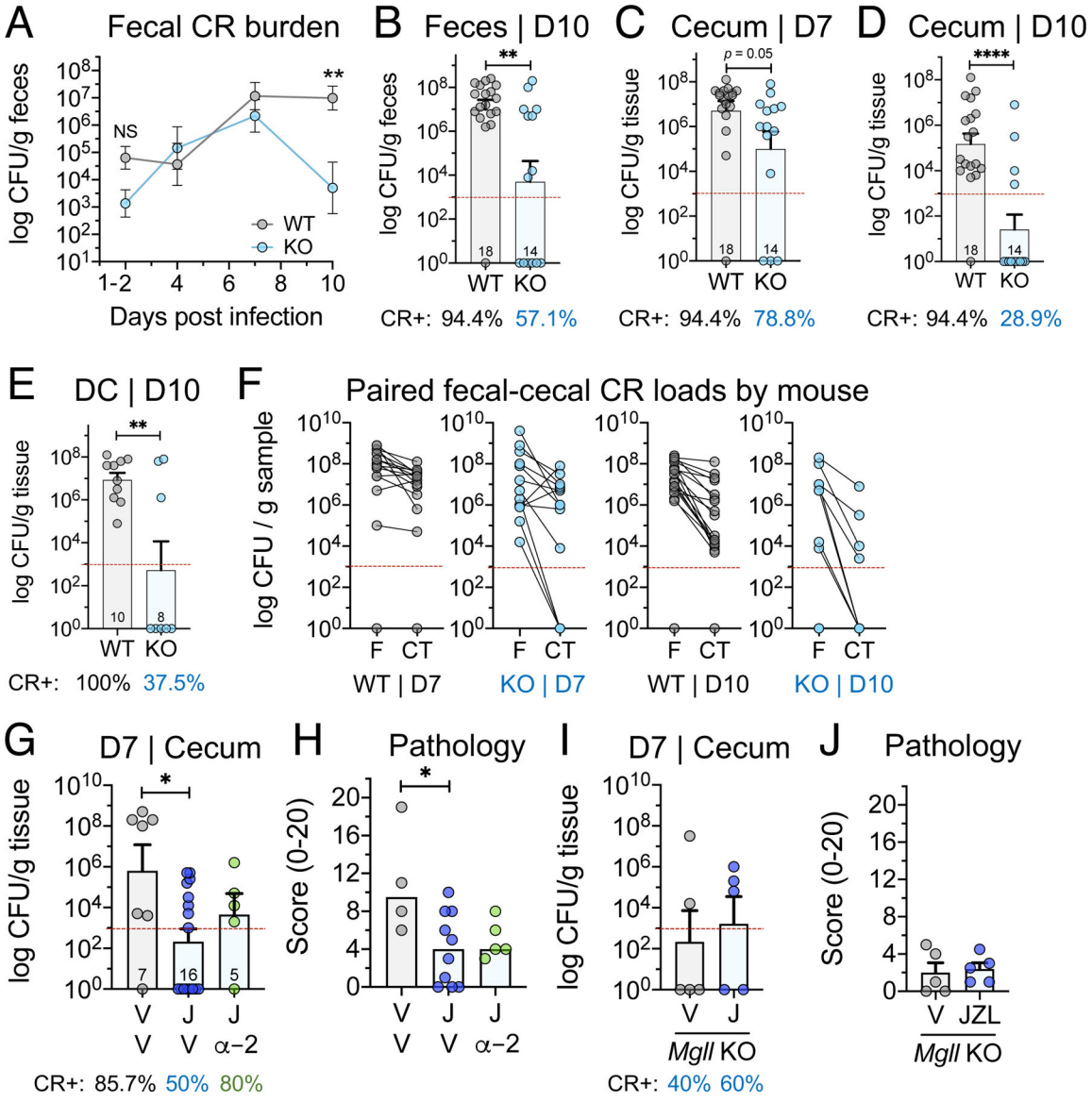

Figure 2. *C. rodentium* Colonization of Intestinal Tissues Is Attenuated in Mice with Elevated 2-Arachidonyl Glycerol Levels

(A) CR burdens in feces collected from *Mgll* WT or KO mice (n = 14–18) at days 1–2, 4, 7, or 10 post-infection.

(B) CR burdens in feces collected from *Mgll* WT or KO mice (n = 14–18) at day 10 post-infection.

(C and D) CR burdens in cecal tissues harvested from *Mgll* WT or KO mice (n = 14–18) at (C) day 7 or (D) day 10 post-infection.

(E) CR burdens in distal colon tissues harvested from *Mgll* WT or KO mice (n = 8–10) at day 10 post-infection. The percentage of mice positive for CR in feces or colon tissues as assessed by bacterial culture is indicated at the bottom of each graph by experimental group.

(F) Paired CR burdens in feces and cecal tissues from the same animal at day 7 or 10 post-infection.

(G–J) Female *Mgll* WT or KO mice were chronically administered i.p.: the *Mgll* inhibitor JZL184 (J) at 16 mg/kg, the cannabinoid receptor 2 inhibitor AM630 (α−2) at 10 mg/kg, or the vehicle control (V) prior to infection with CR. (G) Cecal CR burdens at day 7 post-infection in *Mgll* WT mice administered JZL184, AM630 with JZL184, or the vehicle (n = 5–16). The percentage of mice positive for CR in cecal tissues as assessed by bacterial culture is indicated at the bottom of each graph by experimental group. (H) Combined gross pathology scores of ceca and colons at day 7 post-infection in CR-infected *Mgll* WT administered JZL184, AM630 with JZL184, or the vehicle (n = 4–10). (I) Cecal CR burdens at day 7 post-infection in *Mgll* KO mice administered JZL184 or the vehicle (n = 5). The percentage of mice positive for CR in cecal tissues as assessed by bacterial culture is indicated at the bottom of each graph by experimental group. (J) Combined gross pathology scores of ceca and colons at day 7 post-infection in CR-infected *Mgll* KO mice administered JZL184 or the vehicle (n = 5). All data are represented as either the mean ± SEM (A–E, G, and I) or as the median (H and J). The red dashed line represents the detection limit for quantitative bacterial culture.

p values were determined by Student's unpaired t test (B–E and I), one-way ANOVA (G), Kruskal-Wallis (H), or two-way ANOVA (A). See also Figures S2 and S3.

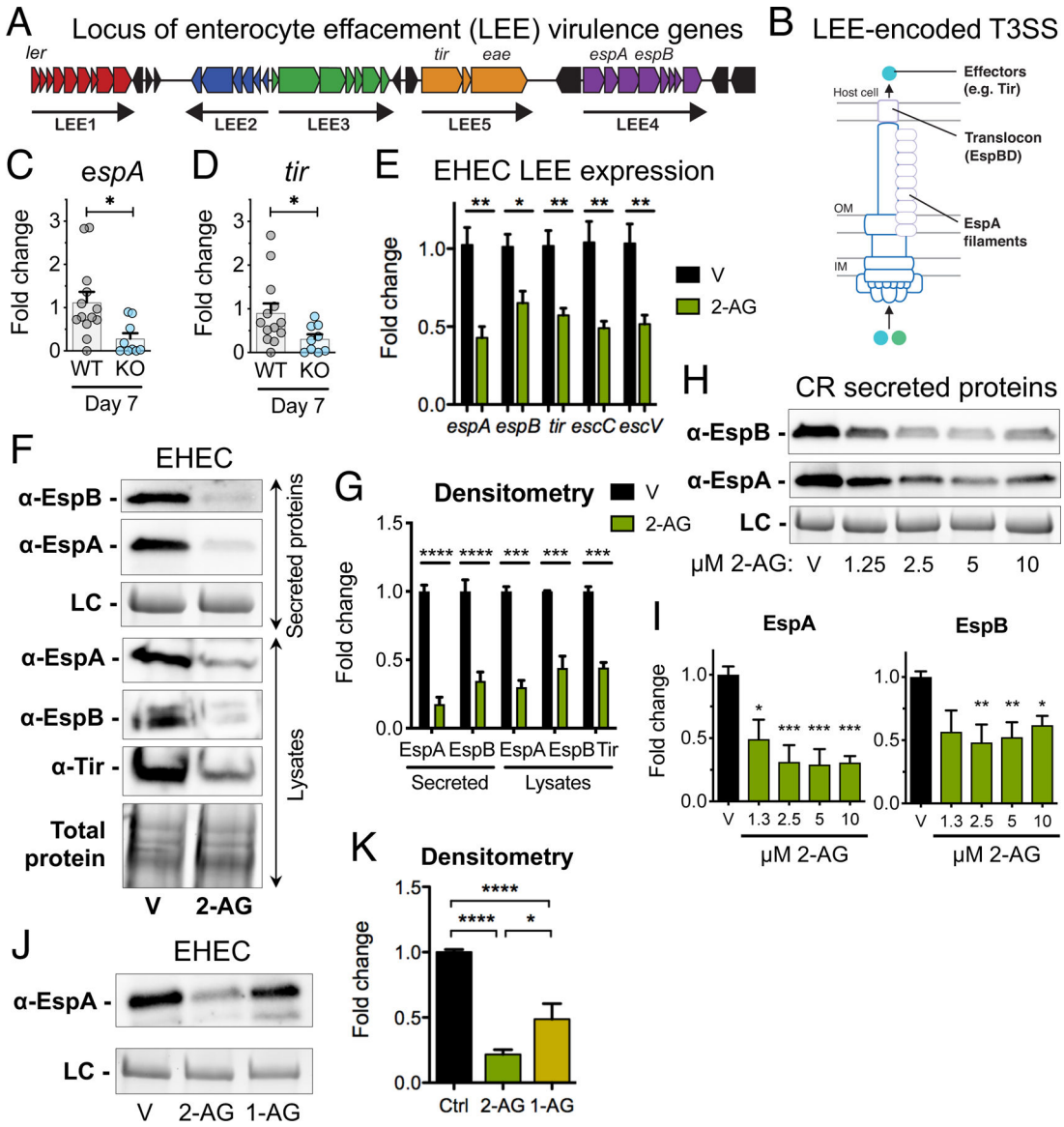

Figure 3. 2-AG Directly Inhibits Virulence Activity in Human and Murine Attaching/Effacing Pathogens

(A) Schematic depicting the genetic organization of the locus of enterocyte (LEE) pathogenicity island that encodes virulence genes essential for intestinal infection in attaching/effacing (AE) pathogens.

(B) Schematic of the LEE-encoded type three secretion system (T3SS) needle apparatus.

(C and D) Relative CR expression of LEE-encoded (C) *espA* and (D) *tir* recovered from cecal contents of infected *Mgll* WT or KO mice (n = 9–13).

(E–K) EHEC or CR were grown microaerobically under LEE-inducing conditions (DMEM-low glucose) in the presence of 2-AG or the vehicle control (V). (E) Relative expression of representative genes from each of the 5 LEE operons in EHEC as assessed by targeted qRT-PCR. (F and G) EHEC secretion and expression of EspA, EspB, and the effector Tir at late-log phase as assessed by western blots. (F) Blots are representative of at least 3 independent experiments. LC, loading control. (G) Densitometry of the data represented in (F). (H and I)

CR secretion of EspA and EspB at late-log phase as assessed by western blots. (H) Blots are representative of at least 3 independent experiments. LC, loading control. (I) Densitometry of the data represented in (H). (J and K) EHEC secretion of EspA in response to 2-AG or 1-AG as assessed by western blots. (J) Blots are representative of at least 3 independent experiments. LC, loading control. (K) Densitometry of the data represented in (J). All data are represented as the mean ± SEM of at least 3 independent experiments.
p values were determined by Student's unpaired t test (C–E and G) or one-way ANOVA (I and K). See also Figure S4.

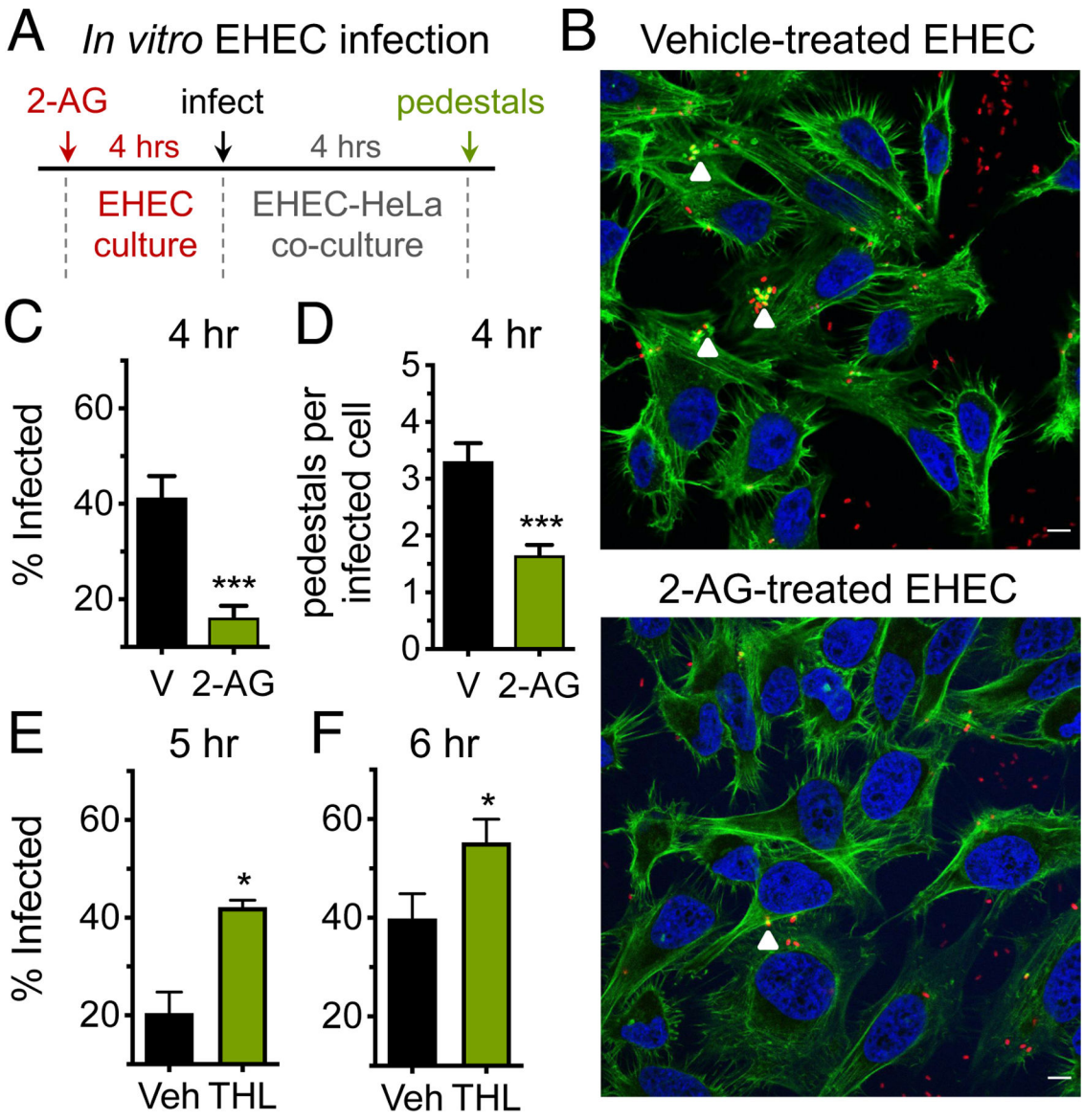

Figure 4. 2-AG Attenuates T3SS-Dependent Pathogenic Interactions between Attaching/Effacing Pathogens and the Host

(A) EHEC was grown microaerobically under LEE-inducing conditions (DMEM-low glucose) with 2-AG or the vehicle control (V). At late log phase, 2-AG- or vehicle-treated EHEC was transferred to a co-culture system with HeLa cells to initiate EHEC infection.

(B) Representative confocal microscopy images of LEE-dependent pedestal formation (white arrow-heads) on epithelial cells by mCherry-expressing EHEC. DNA (blue) is stained with DAPI and actin (green) is stained with FITC-phalloidin. Images at 40×.

(C) Percentage of epithelial cells infected with EHEC pedestals at 4 h post-infection.

(D) Quantity of EHEC pedestals per infected epithelial cell at 4 h post-infection. At least 275 cells in 17 fields at 40× were enumerated for each group.

(E and F) Percentage of epithelial cells infected with EHEC pedestals at (E) 5 h or (F) 6 h post-infection. Caco-2 epithelial monolayers were pre-treated with the DAGL (α/β) inhibitor

tetrahydrolipstatin (THL) or vehicle control (Veh) 30 min prior to infection. At least 400 cells in 20 fields at 40× were enumerated for each group.

All data are represented as the mean ± SEM. p values were determined by Mann-Whitney. See also Figure S4.

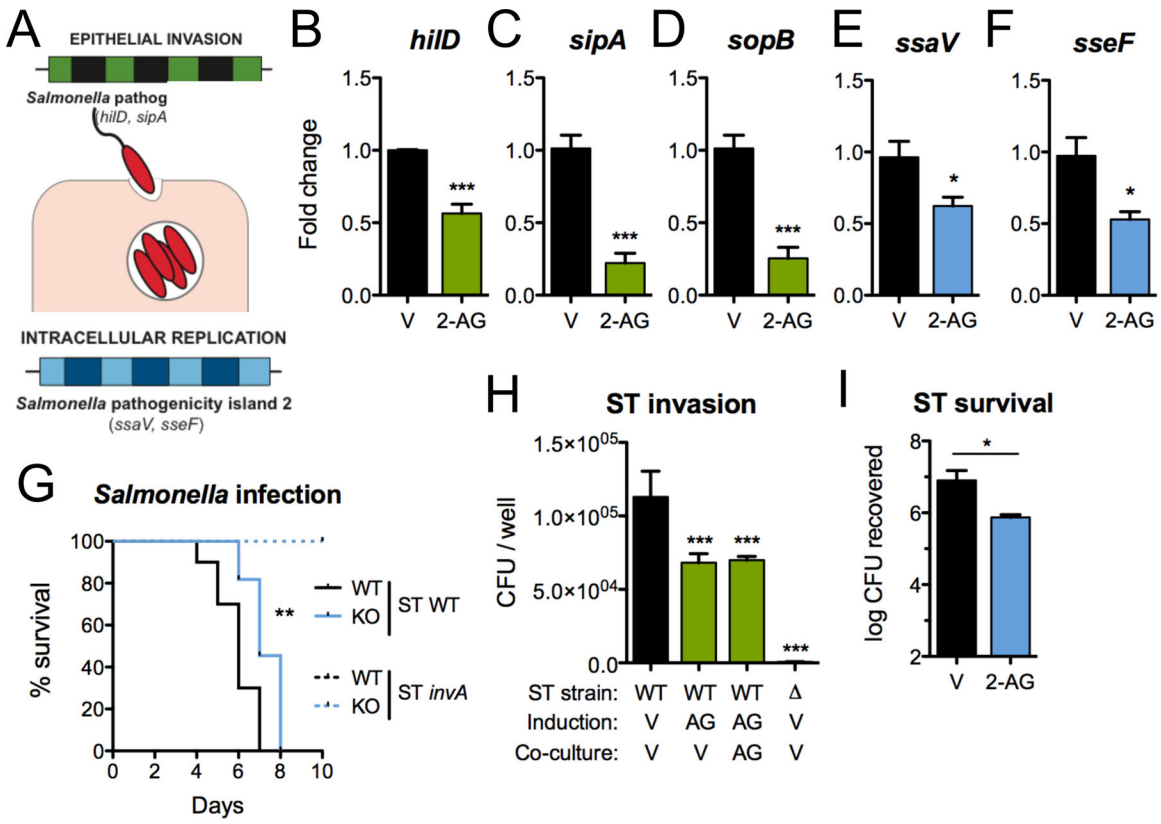

Figure 5. 2-AG Attenuates T3SS-Dependent Pathogenic Interactions between *Salmonella* and the Host

(A) Schematic of the contributions of the SPI-1 and SPI-2 genomic islands to *Salmonella* epithelial invasion and intracellular survival.

(B–D) *S. typhimurium* (ST) was grown aerobically under SPI-1-inducing conditions (LB broth) in the presence of 10 μM 2-AG or the vehicle control (V). (B–D) Relative transcript levels at late-log phase of SPI-1-encoded (B) *hilD*, (C) *sipA*, and (D) *sopB*.

(E and F) ST was grown aerobically under SPI-2-inducing conditions (N9 minimal medium) in the presence of 10 μM 2-AG or the vehicle control (V). Relative transcript levels at 3 h of SPI-2-encoded (E) *ssaV* and (F) *sseF*.

(G) Survival of streptomycin-treated *Mgll* WT or KO mice following infection with ST (n = 10–11 for ST WT, n = 3–5 for ST Δ).

(H) *S. typhimurium* (ST) was grown in the presence of 10 μM 2-AG or the vehicle control (V), and at late log phase, was transferred to a co-culture system with HeLa cells to initiate ST epithelial infection. Quantitative culture of intracellular ST (WT) as a measure of ST epithelial invasion from at least 3 biological replicates. The SPI-1-inactived ST mutant D*invA* (Δ) served as a non-invasive negative control.

(I) Intramacrophagic survival of ST in the presence of 2-AG or the vehicle control (V) as assessed by quantitative culture from at least 3 biological replicates. All data are represented as the mean ± SEM p values were determined by Student's t test (B–F and I), one-way ANOVA (H), or Mantel-Cox test (G). See also Figure S5.

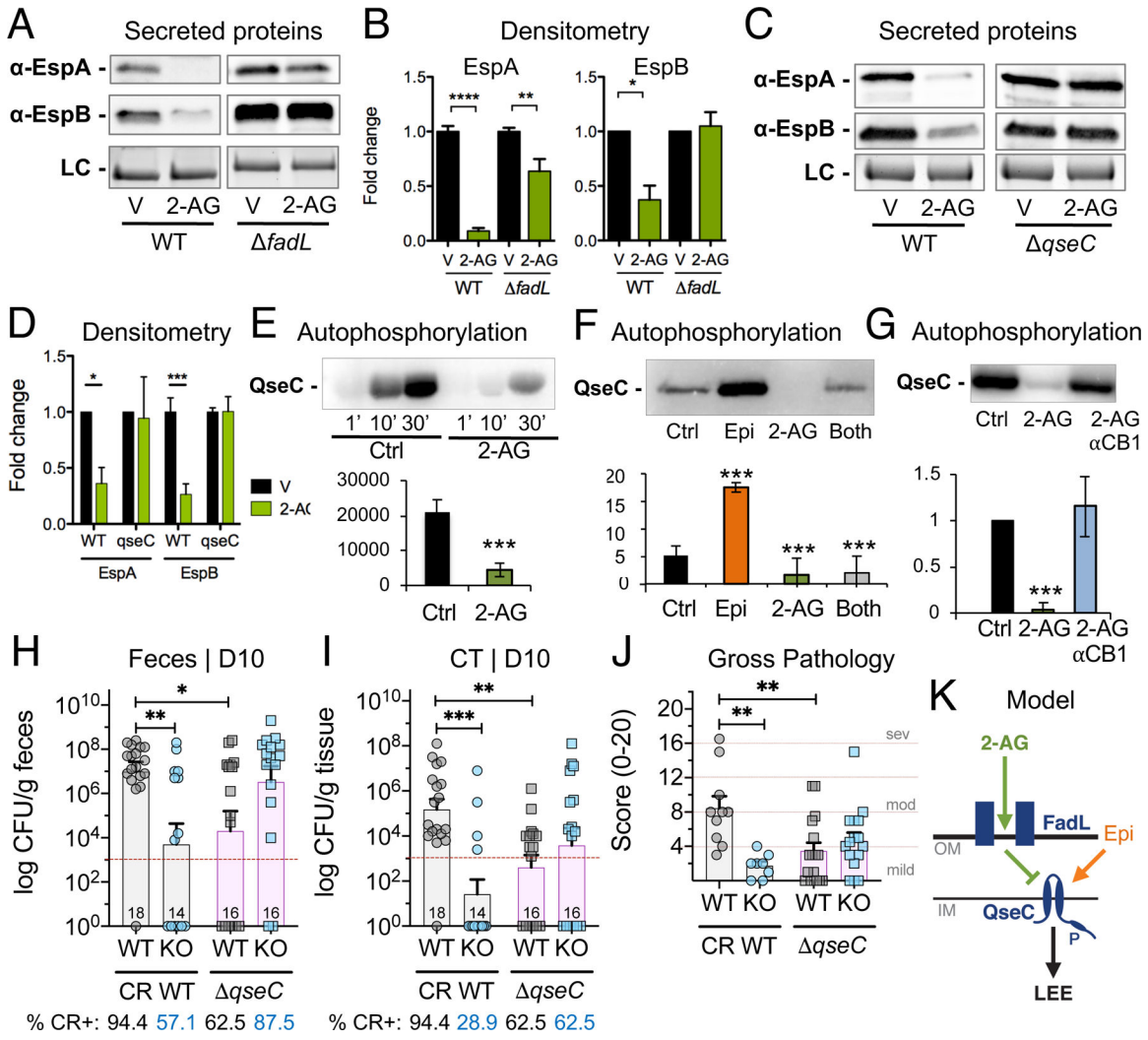

Figure 6. 2-AG Inhibits the Bacterial Receptor QseC to Mediate Its Anti-virulence Effects

EHEC was grown microaerobically under LEE-inducing conditions (DMEM-low glucose) with 10 μM 2-AG or the vehicle control (V).

(A and B) Secretion of EspA and EspB in EHEC WT or Δ*fadL* as assessed by western blots. (A) Blots are representative of at least 3 independent experiments. LC, loading control. (B) Densitometry of the data represented in (A).

(C and D) Secretion of EspA and EspB in EHEC WT or Δ*qseC* as assessed by western blots. (C) Blots are representative of at least 3 independent experiments. LC, loading control. (D) Densitometry of the data represented in (C).

(E) Autophosphorylation of QseC in liposomes in the presence or absence of 2-AG.

(F) Autophosphorylation of QseC in liposomes in the presence or absence of 6 μM 2-AG, 50 μM epinephrine (Epi), or 2-AG and epinephrine (both) after 30 min.

(G) Autophosphorylation of QseC in liposomes in the presence or absence of 6 μM 2-AG, or 2-AG and the CBR1 inhibitor AM251 (antiCB1) after 30 min.

(H and I) CR WT or Δ*qseC* burdens in (H) feces or (I) cecal tissues collected from *Mgll* WT or KO mice (n = 14–18) at day 10 post-infection.

(J) Combined gross pathology scores of ceca and colons harvested from CR-infected *Mgll* WT or KO at day 10 post-infection (n = 8–10 [CR-WT]; n = 16 [CR-*qseC*]).
(K) Schematic of proposed model depicting 2-AG sensing in A/E pathogens. All data are represented as either the mean ± SEM (B, D–I) or as the median (J). The red dashed line represents the detection limit for quantitative bacterial culture. Data from mice infected with CR WT (3 independent cohorts) are depicted in Figure 1, with one cohort run together with CR *qseC*. Three independent cohorts were run for CR *qseC*.
p values were determined by Student's unpaired t test (B, D, and E), one-way ANOVA (F–I), or Kruskal-Wallis (I). See also Figure S6.

KEY RESOURCES TABLE

REAGENT or RESOURCE	SOURCE	IDENTIFIER
Antibodies		
Anti-EspA-polyclonal, rabbit	UT Southwestern, Vanessa Sperandio	N/A
Anti-EspB-polyclonal, rabbit	UT Southwestern, Vanessa Sperandio	N/A
Anti-Tir-polyclonal, rabbit	UT Southwestern, Vanessa Sperandio	N/A
Anti-rabbit-HRP, goat	BioRad	Cat# 1706515
Bacterial and Virus Strains		
EHEC str 86–24	U of Maryland, James Kaper	N/A
E. coli DH5α	UT Southwestern, Vanessa Sperandio	N/A
E. coli TOP10	Invitrogen	Cat# C404052
E. coli BL21 (DE3)	Invitrogen	Cat# C600003
S. enterica serovar Typhimurium SL1344	UT Southwestern, Sebastian Winter	N/A
S. enterica serovar Typhimurium IR715	UT Southwestern, Sebastian Winter	N/A
C. rodentium DBS100	Tufts University, John Leong	N/A
Chemicals, Peptides, and Recombinant Proteins		
Dulbecco eagle medium, high glucose	Invitrogen	Cat# 11965–092
Dulbecco eagle medium, low glucose	Invitrogen	Cat# 11885–084
Heat inactivated fetal bovine serum (FBS)	Thermo Fisher	Cat# 10082–147
Penicillin-streptomycin solution	Thermo Fisher	Cat# 15140–122
LB agar, Miller	Fisher Scientific	Cat# BP1425
LB broth, Miller	Fisher Scientific	Cat# BP9723
Ampicillin powder	Sigma-Aldrich	Cat# A9518
Streptomycin powder	Sigma-Aldrich	Cat# S6501
Naladixic acid power	Fisher Scientific	Cat# BP908
2-arachidonoyl glycerol	Tocris	Cat# 1298
1-arachidonoyl glycerol	Cayman Chemical	Cat# 62150
Anandamide	Tocris	Cat# 1339
Arachidonic acid	Sigma-Aldrich	Cat# 10931
Gibson assembly master mix	New England Biolabs	Cat# M5510A
Indole	Sigma-Aldrich	Cat# I3408
L-(+)-Arabinose	Sigma-Aldrich	Cat# A3256
Isopropyl β-D-1-thiogalactopyranoside (IPTG)	Sigma-Aldrich	Cat# I6758
Phusion High fidelity PCR master mix	Thermo Fisher	Cat# F-531L
Random primers	Invitrogen	Cat# 48190–011
Super script II reverse transcriptase	Invitrogen	Cat# 18064–014
Sybr green master mix	Thermo Fisher	Cat# 4309155
Trizol reagent	Thermo Fisher	Cat# 1559618
dNTP mix 10mM	Invitrogen	Cat# 18–427-088

REAGENT or RESOURCE	SOURCE	IDENTIFIER
AM630	Cayman Chemical	Cat# 10006974
JZL184	Cayman Chemical	Cat# 13158
Chloroform	IBM Scientific	Cat# 67–66-3
Bovine Serum Albumin	Sigma-Aldrich	Cat# A2153
Bio-Safe Coomassie Stain	BioRad	Cat# 1610787
Protease inhibitor cocktail	Sigma-Aldrich	Cat# P8849–5
SuperSignal West Dura Extended Duration Substrate	Thermo Fisher	Cat# 34075
FITC-Phalloidin	Sigma-Aldrich	Cat# P5282
ProLong™ Gold Antifade Mountant with DAPI	Thermo Fisher	Cat# P36931
Tetrahydrolipstatin	Cayman Chemical	Cat# 10005426
AM251	Tocris	Cat# 1117
Ni-NTA beads	Thermo Scientific	Cat# 88221
5 mL disposable columns	QIAGEN	Cat # 1018597
E. coli polar lipid extract	Avanti polar lipids, Inc.	Cat# 100600
N-octyl-β-D-glucopyranoside	Sigma-Aldrich	Cat# O8001
Bio-Beads SM-2 Adsorbent media	Biorad	Cat# 152–8920
n-Dodecyl β-D-maltoside	Sigma-Aldrich	Cat# D4641
Epinephrine bitartrate	Sigma-Aldrich	Cat# 1237000
Adenosine triphosphate	PerkinElmer	Cat# BLU002A250UC
Dithiothreitol (DTT)	Fisher Scientific	Cat# BP172–25
Imidazole	Sigma-Aldrich	Cat# I2399
Formaldehyde	Fisher Scientific	Cat# BP539
2.0-mL Bead Ruptor tubes with 2.8 mm ceramic beads	Omni International	Cat# 19–628
FA (20:4 ω6{$^2H_8$}) fatty acid standard	Cayman	Cat# 9000477
DL-Norepinephrine hydrochloride	Sigma-Aldrich	Cat# A7256
DB-5MS column	Agilent	Cat# 121–5542
Critical Commercial Assays		
RNeasy Power Microbiome	QIAGEN	Cat# 26000–50
RiboPure RNA isolation Kit	Ambion	Cat# 1405072
GenElute Plasmid Miniprep	Sigma	Cat# PLN350–1KT
QIAquick PCR purification kit	QIAGEN	Cat# 28906
Illumina Nextera DNA Library Prep kit	Illumina	Part# 15044223 Rev. B
Illumina ScriptSeq Complete kit	Illumina	BB1224
Deposited Data		
RNA sequencing data	This paper	ENA: PRJEB29880
16*S* rRNA sequencing data	This paper	pending
Experimental Models: Cell Lines		
HeLa cell line	ATCC	Cat# ATCC® CCL-2.1
Caco-2 cell line	ATCC	Cat# ATCC® HTB-37

REAGENT or RESOURCE	SOURCE	IDENTIFIER
J774.1 cell line	ATCC	Cat# ATCC® TIB-67
Experimental Models: Organisms/Strains		
C57BL/6J mice	The Jackson laboratory	Cat# 000664
Mgll$^{+/-}$ mouse breeding pairs	Texas A&M Institute for Genomic Medicine Mouse Repository	N/A
Oligonucleotides		
Primers for qRT-PCR used in this study are listed in Table S2	This paper	N/A
Mgll genotyping primers:	Texas A&M Institute for Genomic Medicine Mouse	N/A
Mgll 5′ F7: GGAAACAGGTTTGTCATGGC	Repository	
Mgll 3′ R1: GCGAGAAACCAGAAGGAGAC		
Primers to amplify V3 & V4 hypervariable region for 16*S* rRNA profiling:	This paper	N/A
16*S* Forward Primer 5′TCGTCGGCAGCGTCAGATGTGTATAAGAGACAGCC TACGGGNGGCWGCAG		
16*S* Reverse Primer 5′GTCTCGTGGGCTCGGAGATGTGTATAAGAGACAGG ACTACHVGGGTATCT AATCC		
Recombinant DNA		
Plasmid pDP151 (constitutive mCherry expression)	UT Southwestern, Neal Alto	N/A
Plasmid pET21a-CpxA	Kumar A 2019, *mBio*	N/A
Plasmid pBAD-QseC-MycHis	Clarke M 2006, *PNAS*	pVS144
Software and Algorithms		
Prism 8 for Mac	GraphPad	N/A
QuantStudio real-time PCR software v1.3	Thermo Fisher	N/A
Image Lab 5.2.1	BioRad	N/A
BBmap software suite	https://sourceforge.net/projects/bbmap/	N/A
Bowtie2	http://bowtie-bio.sourceforge.net/bowtie2/index.shtml	N/A
featureCounts package	https://www.rdocumentation.org/packages/Rsubread/versions/1.22.2/topics/featureCounts	N/A
DESeq2	https://bioconductor.org/packages/release/bioc/html/DESeq2.html	N/A
CLC Bio microbial genomics module	https://digitalinsights.qiagen.com/plugins/clc-microbial-genomics-module/	N/A
Golden Helix Software	https://www.goldenhelix.com/	N/A
Fiji ImageJ	https://fiji.sc/	N/A
MultiQuant 3.0.3. Software	https://sciex.com/products/software/multiquant-software	N/A
MassHunter Software	Agilent	N/A